Final Draft

of the original manuscript

Juarez, T.; Biener, J.; Weissmueller, J.; Hodge, A.M.:

Nanoporous Metals with Structural Hierarchy: A Review.

In: Advanced Engineering Materials. Vol. 19 (2017) 12, 1700389.

First published online by Wiley: 09.08.2017

https://dx.doi.org/10.1002/adem.201700389

Nanoporous Metals with Structural Hierarchy: A Review

Theresa Juarez, Juergen Biener, Jörg Weissmüller, and Andrea M. Hodge*

Prof. A. M. Hodge, T. Juarez Department of Aerospace and Mechanical Engineering, Mork Family Department of Chemical Engineering and Materials Science, University of Southern California, Los Angeles, CA 90089, USA
E-mail: ahodge@usc.edu

Dr. J. Biener Nanoscale Synthesis and Characterization Laboratory, Lawrence Livermore National Laboratory, Livermore, CA, USA

Prof. J. Weissmüller Institute of Materials Physics and Technology, Hamburg University of Technology, Hamburg, Germany, and Institute of Materials Research, Materials Mechanics, Helmholtz-Zentrum Geesthacht, Geesthacht, Germany

Nanoporous (np) metals have generated much interest since they combine several desirable material characteristics, such as high surface area, mechanical size effects, and high conductivity. Most of the research has been focused on np Au due to its relatively straightforward synthesis, chemical stability, and many promising applications in the fields of catalysis and actuation. Other materials, such as np-Cu, Ag, and Pd have also been studied. This review discusses recent advances in the field of np metals, focusing on new research areas that implement and leverage structural hierarchy while using np metals as their base structural constituents. First, we focus on single-element porous metals that are made of np metals at the fundamental level, but synthesized with additional levels of porosity. Second, we discuss the fabrication of composite structures, which use auxiliary materials to enhance the properties of np metals. Important applications of these hierarchical materials, especially in the fields of catalysis and electrochemistry, are also reviewed. Finally, we conclude with a discussion about future opportunities for the advancement and application of np metals.

1. Introduction

The concept of hierarchical organization is ubiquitous, encompassing both deliberately designed structures and natural materials. Examples of ordered hierarchy are most evident in biological systems, where pore networks in trees and bones reduce the density of the structure and provide channels for fluid and nutrient flow, enhancing mechanical properties while adding functionality.[1] Biological systems exploit hierarchy from the nanometer up to the macroscale, with a complex architecture in which the structural elements themselves have structure on a smaller scale.[2]Humans have attempted to mimic advanced biological systems by designing frame structures like the Eifel Tower, but the complexity that can be found in natural materials, such as bamboo, has yet to be realized.[3] There may be opportunities in reproducing these types of geometries in man-made materials, where hierarchy is found in the length scales occupied by structural features, such as tiered porosity in single element materials or the spatial distribution of elements in composites. However, this requires the development of new strategies for advanced materials design, specifically the appropriate preparation procedures and an understanding of the effects of hierarchical structure on functional properties. Advances in metal or ceramic deposition methods, templating, and dealloying methods, have made it possible to produce hierarchical structures in a variety of elements and configurations. This review focuses on hierarchy in porous materials that include characteristic pore sizes down to the nanoscale. Specifically, we consider materials in which the smallest and definitive length scale is occupied by nanoporous (np) metalmade by dealloying. Examples of as-dealloyed np topologies are shownat the center of Figure 1. Alternative processing methods that can produce additional levels of tunable structure in single-phase materials (left of Figure 1) or in composites (right of Figure 1) are also reviewed.

2. Background

2.1. Materials with Multiple Length Scales, Stochastic versus Periodic

Metals with pore sizes on the order of nanometers to millimeters are used in a variety of structural and functional applications such as heat exchangers,[4,5] filters,[6,7] energy absorbers,[8,9] and

catalysts.[10,11]Their key benefits include a large amount of internal surface area and high thermal and electrical conductivity.[12,13] In particular, the automotive, construction, and aerospace industries are interested in foams as lightweight structural components to maximize strength to weight ratios, impact absorption, and vibrational damping.[14,15]

Incorporating additional length scales or architectures can significantly improve the performance of materials. A prime example is the design of sandwich panels and their core structure to improve both mechanical properties and heat transfer properties when a fluid flows through the panel.[16–18]

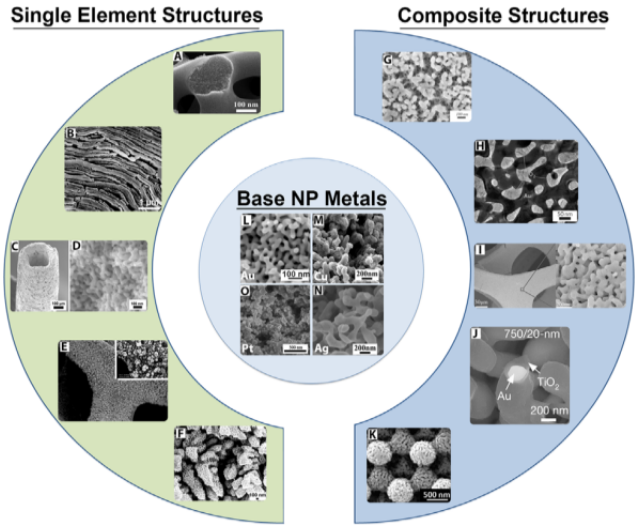

Figure 1. Schematic representing various hierarchical structures in single element np materials (a–f) and composite structures (g–k) that are based on np metal morphologies (l–o) produced by dealloying. f, b, and j) reproduced from ref.[105,122,206] respectively. Copyright 2009, 2012, 2015 American Chemical Society. m, l, and c & d) reproduced with permission from ref.[68,74,85] respectively. Copyright 2011, 2006, 2015, John Wiley and Sons. e) adapted from ref.[105] with permission from Springer. Copyright 2016. n, i, and g) reprinted from ref.[70,138,213] respectively, with permission from Elsevier. h) adapted with permission from Macmillan Publishers Ltd: Nature Nanotechnology, ref.[126] copyright 2011. k and o) reproduced from ref.[137,214] with permission of The Royal Society of Chemistry.

Examples of different core architectures include traditional foam core, honeycombs, or truss structures with periodic architecture. The variety of available core designs and numerous material options allows for the optimization of these metal cellular structures for applications in the aerospace and automotive industry.[16,19] Cellular materials can be classified into two broad categories, stochastic and periodic, see the examples in Figure 2. Stochastic materials (Figure 2a–c) have random pore distributions, where various degrees of short-range order and pores size distribution can be found. Periodic structures (Figure 2d–f) have a base cell that is repeated in two dimensions, such as the honeycomb in Figure 2f, or in three dimensions, such as the trusses in Figure 2e.[14,15,20] Each category is associated with distinct mechanical properties as well as differences in relative density and production effort or cost. The use of various synthesis methods can also yield characteristic pore and ligament sizes from the macroscale down to the nanoscale. Both stochastic and periodic materials can be fabricated with a wide variety of base metals, from aluminum to titanium, and with closed or open porosity. The distinction between closed and open porosity is crucial. For instance, the latter implies permeability to fluids, typically along with a lower density.[14,21] When evaluating the mechanical properties of stochastic and periodic structures, one finds that for a given relative density, ordered porous structures have superior load-bearing properties when compared to their stochastic counterparts.[22]

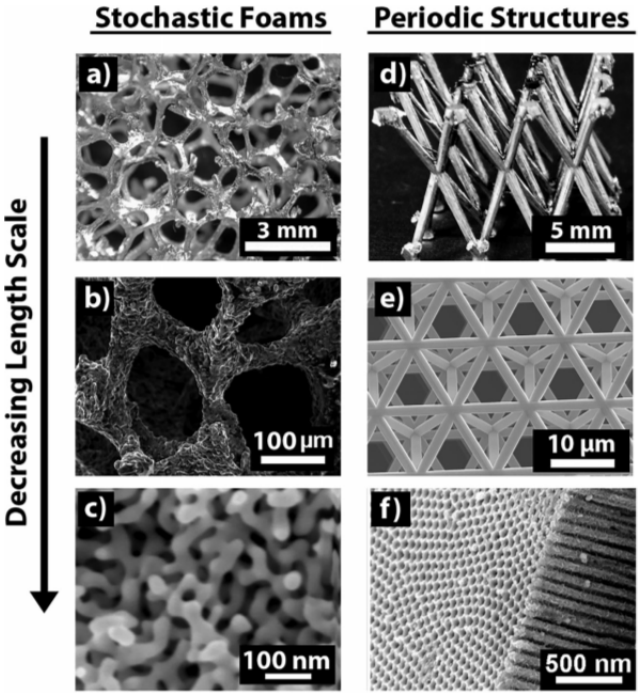

Figure 2. Classifications of cellular materials as either stochastic a–c) or periodic d–f), with cellular features from the macroscale down to the nanoscale for each type of cellular structure. f) adapted with permission from ref.[215] Copyright 2015 American Chemical Society.

This is because periodic trusses or networks are typically stretch-dominated materials when loaded, whereas random networks are bending-dominated.[23] Additionally, closed-cell materials usually have an increased relative modulus for a given relative density, making them more desirable for load bearing applications.[15,22] Key advantages of using open porous structures for practical applications include mass reduction and the large accessible surface area.[14,15] This, for example, is important for catalysis[24] or applications requiring cooling, since both the rate of product formation and heat transfer increase with the available surface area.[25,26] For the purposes of this review, we are only interested in open cell structures, since their large accessible surface area enhances the potential for the added functional applications, such as catalysis and energy storage, that are discussed in Section 4. The mechanical behavior of stochastic porous solids, as well as ordered cellular materials such as truss structures, are described in the seminal work on themechanics of cellular solids by Gibson and Ashby.[27] This work shows that the strength of porous solids is fundamentally governed by the relative density of the material. By contrast, the Gibson–Ashby approach predicts that mechanical properties do not depend on the cell size, except for a certain sensitivity of strength to the ratio of the cell wall thickness to cell length.[27] It is therefore unexpected that the properties of the np metals discussed in this review do not scale according to the Gibson and Ashby equations.[28–30] The interest in this issue can be traced back to early experiments revealing drastic changes in strength when the struts or ligaments of np gold are varied while maintaining the same relative density.[29–40] Studies on the mechanical behavior of np metals are numerous and suggest interesting size effects. Still, the influence of structural hierarchy on the plastic yield and flow behavior in these materials remains to be clarified. By contrast, hierarchy from the nm scaleup has beenthoroughly addressed by theory analyzing the fracture strength of biological materials.[41,42] Therefore, this review will instead focus on the relevance of hierarchy for functional applications and on emerging preparation techniques.

2.2. Fabrication of Macro-Foams to Nanoporous Materials: Basic Concepts

The origins of the earliest made porous metals for commercial use can be traced back to the 1920s, when French scientist De Meller described a process of injecting gas into molten metals, now common practice for producing metallic foams.[43] The injected gases develop into bubbles that become pores.[9] Alternative processing methods use powder sintering, where fine metal powders are compacted with a metal hydride and heat-treated near the melting temperature of the metal. This releases gas from the hydride and forms

pores in the soft metal.[9] One approach to enhance the properties of metal foams includes careful selection of the base metal alloy to produce strengthening intermetallics.[44] It is important to note that these foaming techniques form mm sized pores and are thus generally limited to macroscale porosity (Figure 2a). Furthermore, these techniques offer limited ability to impart additional levels of structural hierarchy other than material characteristics such as grain size and dispersed particles. An established technique to create microscale porous foams involves the deposition of metal onto a polymer scaffold and subsequent etching or burning out of the polymer, which results in a hollow strut metal foam (Figure 2b). Unlike the foaming methods, this approach can be tailored by using engineered microlattice polymer scaffolds and controlling the amount of metal deposited onto the scaffold, allowing some influence on the wall thickness.[45,46] Thus far, traditional preparation methods for metal foams have not been able to achieve cell sizes below the micron scale.

Recent fundamental work on the synthesis, properties, and applications of nanoporous metals with feature sizes in the tens of nanometers, has started a research field focusing on a new class of porous metals. As a key advancement, dealloying has emerged as a synthesis route toward monolithic np metals. Dealloying combines high structural definition and morphological control with compositional flexibility and a high level of reproducibility. Np metals made by dealloying lack the cell structure that is characteristic of materials produced by foaming. Instead, this new class of materials is characterized by an interconnected network of nano- or microscale ligaments interpenetrated by a contiguous (open) array of pore channels. Like their macroporous counterparts, nanoscale networks exhibit high stiffness. However, a distinctive feature of np metals is their drastically increased surface area. The specific surface area (per volume or per mass) scales inversely with the feature size. The large surface area that can be achieved with nanoscale pores makes dealloyed np metals highly attractive when function derives from properties or processes at the material surface, for instance in catalysis,[11,47–50] sensing,[11,51,52] and actuation.[53,54] The fundamental mechanisms of dealloying to produce np metals have been explored since the early 20th century.[55,56] Examples for more recent studies can be found in the work by Pickering and Swan,[57,58] Forty,[59] as well as Newman and Sieradzki.[60,61] The present understanding of dealloying was established when Sieradzki, Erlebacher and coworkers reproduced key experimental observations in a simple atomistic simulation scenario.[62–64] Essentially, dealloying is the selective electrolytic corrosion of a master alloy that is a solid solution or compound of a more noble element (MNE) and a less noble element (LNE). Its central process is the corrosive dissolution of the LNE in free-corrosion dealloying, through the immersion of the alloy in a corrosive medium, or in electrochemical dealloying, by the combined action of chemical and electric driving forces for dissolution.[32] In the latter case, the electrode potential affords control of the rate of LNE removal.[61,62] More recently, liquid metal dealloying has been employed where one or more components of the starting alloy selectively dissolve in molten metal.[65] It is important to realize that the characteristic pore/ligament structure of np metals made by dealloying is not related to any similar structure in the master alloy. Instead, the nanoscale structure is formed by self-organization during the corrosion process. The underlying atomic-scale processes are the dissolution of the LNE and surface diffusion of one or both elements along the metal-solution interface. This results in monolithic bodies with a bicontinuous structure of pore and solid. The uniform 3D morphology is shown in Figure 3. The interpenetrating networks of pore channels and ligaments are not periodic, yet each individually exhibits a high connectivity and well-defined characteristic feature size and spacing between neighboring elements. Important parameters in dealloying are the parting limit and the critical potential for dealloying.[66,67] The parting limit marks the minimum concentration of LNE (or maximum concentration of MNE) which is required for corrosion to proceed throughout the bulk of an alloy rather than being arrested by passivation. For example, studies suggest a parting limit of approximately 45 at% Au for Ag–Au alloy.[66] In electrochemical dealloying, the critical electrode potential, Ec, again refers to a criterion for achieving bulk corrosion. This parameter is composition dependent. For example, in Ag–Au alloys, Ec increases with increasing Au content. The dealloying process can be applied to other solid solutions for the synthesis of np-Cu,[68] Ni,[69] Ag,[70] Pd,[71] and Pt.[72] Au is most studied as the material of choice due to its chemical stability and the availability of established dealloying protocols for control and reproducibility of the nanoscale morphology. For a detailed overview of the present understanding of dealloying and porosity evolution, we point the interested reader to a recent review by McCue and Erlebacher.[73] The length-scale most typically associated with as-dealloyed np gold is about 40–50 nm, but these dimensions depend on the metal and they can be altered by adjusting master alloy composition or dealloying parameters to reduce the ligament size to _5nm.[74–76] The scanning

electronmicroscope (SEM) image inFigure 3a shows a np-Au foam made by free corrosion in nitric acid while Figure 3b shows the structure produced from the same alloy but using electrochemically driven dealloying in 1MHNO3 and 0.01M AgNO3. The impact of different popular dealloying scenarios in aqueous solutions – free corrosion in HNO3 versus electrochemically assisted corrosion in HNO3 or electrochemical corrosion inHClO4 – is explored in the comparative study in ref.[77]

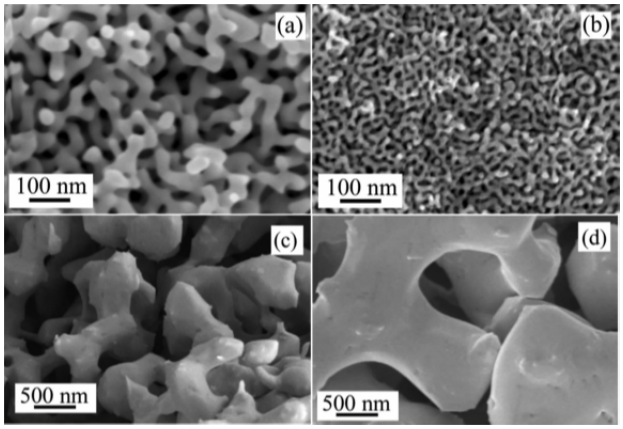

Figure 3. SEM images of np-Au foam prepared by a) free corrosion and b) electrochemically driven corrosion. SEM images of free corrosion samples after 2 h heat treatments at c) 400 _C and d) 600 _C. Reprinted with permission from ref.[74] Copyright 2006 JohnWiley and Sons.

Coarsening heat treatments afford increased ligament sizes, up to the micron scale.[74] For instance, a 2 h heat treatment at 400 _C can double the ligament size (Figure 3c). Higher temperatures and longer heat treatments can yield substantially larger ligaments, such as those in Figure 3d, after 2h at 600_C. Heat treatment protocols by other authors differ, see for instance ref.[78] The ease with which one can alter the ligament size is advantageous since it allows for tuning of properties that depend on size or specific surface area, such as the mechanical strength.[28,35,40,74] Thus far, the field of np metals has grown to encompass a wide range of materials and functionalities or prospective applications. Key aspects of the properties and applications of np gold, as the most intensely studied np metal, are treated in the book edited by Wittstock et al.[79] The more recent and detailed literature is extensive, therefore only a fraction of it can be referenced in this work. Here, special attention is given to studies that have expanded the achievable configurations and applications of np metals by adding structural hierarchy. For clarity, the following definitions are followed in this review. Structural hierarchy is considered to imply organized features on distinct length scales, especially when the elements of the structure at one scale themselves have structure at a smaller scale. Some materials discussed in this review have hierarchical porosity and others have hierarchy that is related to the spatial distribution of the solid phase. Bimodal refers to the presence of two distinct characteristic length scales. When applying the term to hierarchical structures in this review, we imply self-similarity of the pore structures on two distinct length scales. Networks are interconnected arrays of linear features, forming continuous pore or solid pathways. Single element materials are composed of only one element or base np material. Finally, composites are named in the traditional sense, where materials incorporate a combination of constituent materials or elements that are not alloys.

3. Synthesis of Nanoporous Materials with Hierarchy

3.1. Hierarchical and Multimodal Structures

Materials with multiple levels of porosity or hierarchal elements can be achieved by numerous methods, including the use of 3D-printed polymer structures as scaffolds for material deposition, generating more complex architected structures.[45] Etching (or retention) of the polymer after the coating extends the achievable properties of the overall structure, based on the intrinsic properties of the base materials.[80] In a similar manner, using np materials as a base constituent has its own advantages, namely the scalability and the enhancement in surface area. These two main methods (dealloying and templating) for achieving np

materials with multimodal porosity are explored below with consideration for the nuanced approaches toward realizing these unique materials in multiple configurations.

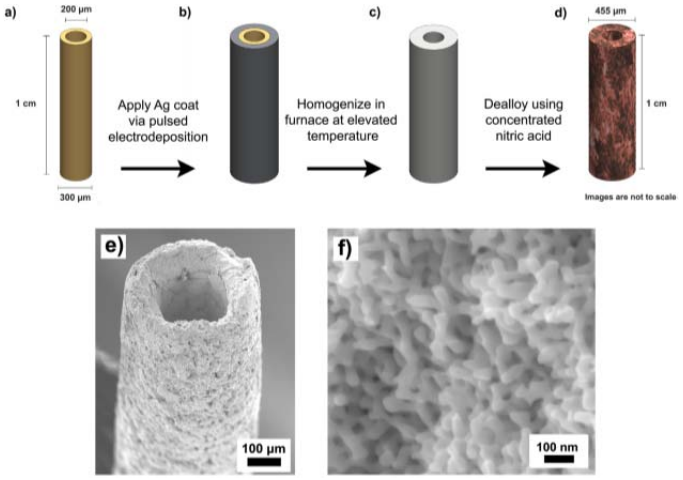

Figure 4. Schematic representation and cross-sectional images for the processing of nanoporous gold tubes. Fabrication begins with a base Au tube a) that is coated with a layer of Ag via electrodeposition b). The layered tube is then homogenized in a furnace c) and then dealloyed to produce a nanoporous Au tube d). SEM images for the tube and the embedded np ligaments are shown in e and f). Adapted with permission from ref.[85] Copyright 2015 John Wiley and Sons.

3.1.1. Templating

While Ding et al.[81] developed the first bimodal np-Au in thin foil form, Nyce et al.[82] developed the first 3D hierarchical bulk np-Au samples with two distinct length scales of porosity using a combination of templating and dealloying. Ag/Au polystyrene (PS) core-shell particles were first prepared by electroless deposition of Ag and Au on PS spheres followed by casting to obtain a monolithic 3D bulk sample, which was then heat treated to remove the PS template while simultaneously alloying the Ag/Au layers. Finally, dealloying transformed the hollow Ag–Au alloy shells of the structure into hollow np shells showing the typical bicontinuous morphology of np Au. The 200nm thick shell wall survived dealloying without crack formation despite the low pre-dealloying Au content of only 15 at%. In general, hierarchical structures[83] and low-dimensional nanoscale objects[84] seem to be more resistant to stress induced cracking than uniform bulk samples that tend to disintegrate during dealloying of low Au content alloys. This type of templating and homogenization of the structures was expanded upon in a study by Juarez and Hodge, where the overall higher order structure was in the form of hollow tubes approaching the centimeter length scale in the largest dimension.[85] The processing steps for this method are shown in Figure 4. First, a hollow Au tube is coated with Ag followed by a heat treatment to form the alloy. The np morphology was then introduced by free corrosion in concentrated nitric acid, resulting in a structurally stable fully np-Au tube. Alternatively, templating can be achieved through electrodeposition of metal into predetermined areas defined by masking. In this sense, Ag–Au nanowires can be made by electroplating the alloy into the nanopores of a suitable template. The alloy nanowires are stripped from the template and dispersed on a substrate, then dealloyed to form np wires (Figure 5a).[86,87] The same idea was applied to develop arrays of nanotubes with np walls, as shown in Figure 5b, and porous Pt-Co nanowires.[88,89] Still, the fabrication of these rods through mesh templating limits the length of the nanowires to the thickness of the resist used to mask the plating channels. The length of the potential nanoarrays was increased by a method for the electrodeposition of Au–Cu onto a patterned silicon substrate. The substrate was made conductive by a vapor-deposited Au seed layer.[90] The resulting patterned structure consists of one-dimensional lines with np structure. More recent work has demonstrated centimeter long np nanowires developed by first sputtering Au–Cu on a rotating silicon substrate with 120nm wide nano-patterned grates and a length of a few centimeters. Rotating the structure with the grates perpendicular to the target throughout sputtering develops the circular cross-section of the rod. The sputtering was followed by electrochemical dealloying of the patterned nanowires resulting in the structures shown in Figure 5c and d.[91] Aside from 2D nanowire arrays, it is also possible to fabricate

hierarchically structured 2D np-Au opal films by electrodepositing a Au–Ag alloy into a silica inverse-opal template. The final np-Au opal structure (Figure 6) is obtained by removing the silica template with an HF etch, followed by free corrosion dealloying in nitric acid.[92] The overall structure of the hierarchical film is displayed in Figure 6c; the smallest pore spacing inside the opals was approximately 10 nm. The opals themselves were approximately 400nm in diameter with an interstitial spacing of 40–100 nm, where the larger gaps in the structure are a result of opal shrinkage during dealloying. Overall, the film is about 2 mm thick and attached to a substrate. Thus far, this type of material, like the shorter nanowires, has not been synthesized in bulk quantities. Templating and dealloying are methods that can be used in combination to incorporate porosity and control of the overall structure of the final material, such as the 1D nanowires, 2D opal structures, and the 3D bulk materials discussed in this section. The use of templates, however, increases the number of synthesis steps required to produce these intricate structures. While templating is necessary when a specific shape is desired, multiple length scales can also be implemented by other methods relying on electrochemistry or the initial microstructure of the precursor alloy which will be discussed in the next section.

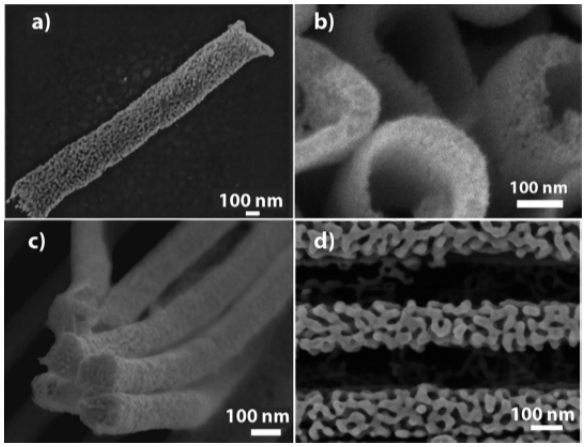

Figure 5. Various nanowire structures ranging from short np wires[86] a) to np nanotubes[88] b) to long nanowires fabricated on silicon patterned substrates c and d).[91] Adapted with permission from ref.[86,88,91] Copyright 2003, 2008, 2016 American Chemical Society.

3.1.2. Dealloying

The earliest example of a hierarchical structure based on np metals, with distinct length scales of self-similar porosity, is from Ding and Erlebacher.[81] The ligaments of this material are composed of smaller ligaments with the same characteristic shape. This architecture was realized by depositing Ag onto a previously dealloyed and subsequently annealed 1 mm thick Au–Ag leaf, with ligament diameters in the range of 100 nm. After Ag deposition and annealing to form an alloy, another dealloying step is performed, resulting in formation of the bimodal pore size structure shown in Figure 7a.[81] The uniform deposition of Ag inside the np-Au structure was achieved by the development of a new gas-liquid interface electroless plating technique that takes advantage of the tendency of np-Au leafs to float on aqueous solutions and therefore requires the film to be thin. While the above concept is limited to the preparation of hierarchical structures in the form of thin films, Qi and Weissmüller demonstrated a dealloying protocol that yields selfsimilar nested networks on different length scales in the form of three-dimensional bodies.[83] They developed a method to electrochemically dealloy a high LNE alloy (Ag95Au5), while retaining enough Ag content to approach the parting limit of the Au–Ag alloy and produce the characteristic np-Au ligament morphology. Coarsening of the initial dealloyed materials increased the ligament size from _16 to _200 nm, similar to the case of np-Au. The key finding in this study is that the characteristic porous structure can be achieved without fully leaching out the Ag, allowing for annealing and a second dealloying step, producing a nested structure like that shown in Figure 7b, with both a higher and lower level of porosity. This sequential dealloying process was later applied to porous sheets of a Ag–Au alloy to generate tri-modal porous structures.[93] Qiu et al.[94] also exploited the difference in electrochemical behavior between elements in a study, where the difference in corrosive

behaviors between Cu and Mn can be used to develop a nested Ni pore structure from a Mn–Cu–Ni alloy. Their study followed the same steps as Qi and Weissmüller, where the precursor alloy was first dealloyed, the ligaments coarsened, and then a final dealloying achieved the second level of porosity. However, the corrosive environments were varied in each dealloying step so that only Mn was removed from the alloy in the first step and Cu was leached in the second. There are many publications where dealloying is applied to master alloy samples which start out with a multiphase microstructure that is created during solidification. The dealloying then works differently on the separate phases, and the coarser microstructure from solidification later coexists with the finer microstructure created by dealloying. When carefully designed and controlled, solidification strategies can result in highly ordered structures with well-defined structural length scales, see ref.[95] Another example of multiphase precursors is demonstrated by the dealloying of Pd–Al alloys produced by spark plasma sintering to make hierarchical np-Pd. A bimodal porous structure is developed in regions where the microstructure is heterogeneous due to the different chemical activities for Al and PdAl3 phases.[96] In regions where both phases are present, a bimodal structure is formed, whereas in regions with only PdAl3, a monolithic porous structure is formed. The regions rich in Pd produce ligaments as small as 7 nm, and the regions rich in Al produce larger pores (_200 nm) with embedded smaller pores due to the PdAl3 phase.[96] Note that doping a precursor alloy with a more noble and low mobility element, such as Pt or Pd, can be used to reduce the size of the np ligaments in single or bimodal materials because of the slower surface diffusion of the more noble element.[75,97–99] Hierarchical np-Pd has also been generated by the electrochemical dealloying of a Pd–Ni–P metallic glass.[100] An early study that showed clear evidence for the benefits of using two-phase starting alloys was by Jin et al.[101] In their study, the solidification of a Pt–Ag master alloy led to Pt-rich dendrites, which resisted corrosion during later dealloying. The dendrites that remained embedded in the nanoporous matrix acted as efficient crack stoppers, substantially enhancing the toughness. In addition to the studies discussed in detail above, several Al alloys, where the Al is removed during dealloying, have been exploited to generate bimodal materials. These include multiphase alloys, including Ni–Al,[102] Al–Cu,[103,104] and Al–Au,[105,106] as well as ternary alloys such as Al–Pd–Au[107] and Pt–Ti–Al[108] that generate binary alloy np materials. In the two latter studies, Al was first dealloyed in NaOH or NaOH/HCl and the more noble elements were removed with nitric acid. Further studies, using multiphase or multi-element alloys for dealloying multimodal porosities can be found in the following references.[109–112] Hierarchical foams can also be made by dealloying preformed, multiphase grain structures within percolation thresholds. Cox and Dunand formed macro/microporous Au–Ag foam by mixing salt into a metal powder pack before compression and sintering.[113] The salt was dissolved in water, which produced large block-shaped macropores, while micropores were developed from the gas expansion of water vapor trapped in the powder compact. This structure is shown in Figure 8. The sintering process alloyed the Au and Ag powders, resulting in a Au19Ag81 at% alloy with graded porosity. The final tier of structure, nanoporosity, was added by dealloying in nitric acid.

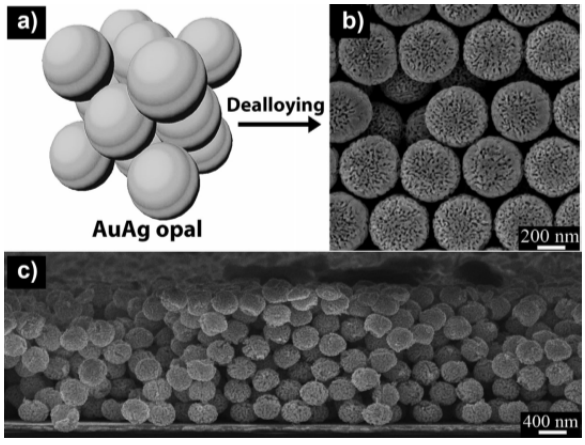

Figure 6. Alloy opal structures a) are dealloyed in nitric acid to develop a porous opal structure b). The overall film structure c) is about 2mm thick. Adapted with permission from ref.[92] Copyright 2012 American Chemical Society.

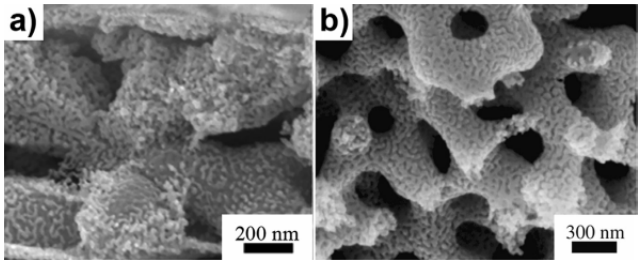

Figure 7. a) Nested np structure generated by depositing an alloying element into a np metal followed by diffusion and dealloying.[81] b) Nested np metal by two-step dealloying of an alloy with abnormally high LNE content.[83] Reproduced with permission from ref.[81] Copyright 2003 American Chemical Society.

Preexisting commercial macroscopic foams can also be manipulated to exhibit nanoporosity. Roughening the surface of commercial Cu foams using electrodeposition and electrochemical dealloying develops a nanoporous layer on the foam surface.[114] This is accomplished using a single aqueous electrolyte solution, where a Ni–Cu alloy is deposited onto a macroporous Cu foam and the Cu is selectively etched during dealloying from both the alloy coating and the pure Cu cell walls underneath. Undercutting of the Ni–Cu film results in the removal of the Ni components, leaving a roughened np layer of Cu on the surface of the walls. Both the number of deposition/dealloying cycles, as well as the time duration for the dealloying pulse can control roughness.[114] In other studies, a combined Gasar and dealloying process fabricated np Cu rods. The Gasar process, that consists of melting a material in a gas atmosphere to saturate it with hydrogen followed by directional solidifying under strictly controlled thermodynamic and kinetic conditions, generates rods with tubular pores oriented along the length of the cylinder.[115] The method was used to develop Gasar Cu-34.5 wt% Mn alloys that then were dealloyed under free corrosion conditions. The resulting bulk samples exhibited both the longitudinal pores from the Gasar process, but also lower level nanoporosity from dealloying of the constituent alloy.[116,117] The material is shown in Figure 9. The initial microstructure of the alloy before selective dissolution can also impact the overall structure of the material. Channeling contrast in focused ion beam imaging[118] and later electron backscatter diffraction imaging,[40,119] showed that nanoporous gold inherits the polycrystalline microstructure of the master alloy, with perfectly coherent crystallites tens of micron in size, in spite of the underlying nanoporosity. Depending on the processing of the master alloy, its grain boundaries can either be completely dissolved to form a gap or can be continuous across the boundary.[120,121] Obviously, mechanical integrity and, even more so, good mechanical behavior under load makes it mandatory to avoid weakening of the porous structure at grain boundaries. Dealloying protocols for Ag–Au and Cu–Au can be tailored to achieve this, as is evidenced by transgranular fracture, as opposed to intergranular fracture along grain boundaries.[33,121] In some instances, it was deemed advantageous to accept the extreme brittleness that comes from preformed cracks at grain boundaries to achieve multiphase microstructures. Thus, Detsi et al.[122] found that a combination of rolling, from 5mm to submillimeter material thickness, and heat treatment of the master alloy can generate features in the microstructure (Figure 10a) that lead to de-cohesion along planar faults during dealloying. Stacked microlayers of np-Au resulted (Figure 10b), where a length scale is described by the layer thickness and another by the ligament size.

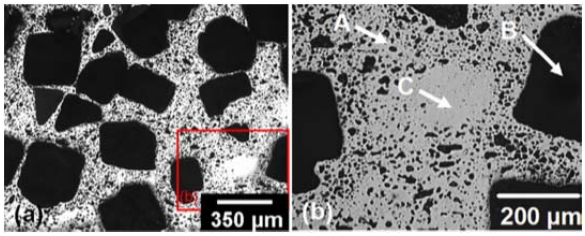

Figure 8. Cross-section of alloy foam before dealloying. a) Large block shaped macropores from salt removal. b) Enlarged area showing micropores from gas expansion. Reprinted from ref.[113] with permission from Elsevier.

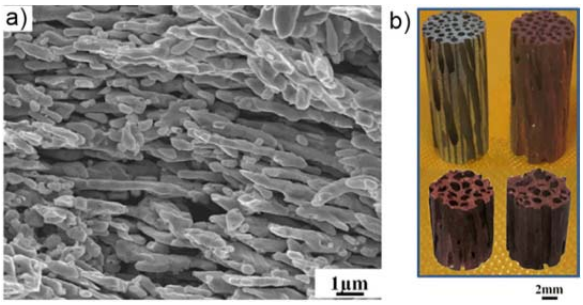

Figure 9. Bimodal Cu rods developed by a combination of the Gasar and dealloying processes to produce nanopores a) within longitudinal pores b). Adapted from ref.[116] with permission from Elsevier.

3.2. Composite Structures Based on Nanoporous Metals

In this section, synthesis methods for incorporating secondary or tertiary materials for auxiliary hierarchy are reviewed, particularly deposition methods that add an additional layer of material onto a np metal surface. Synthesis techniques to develop functional np metal films on larger structures, as well as hierarchical alloy materials, are discussed.

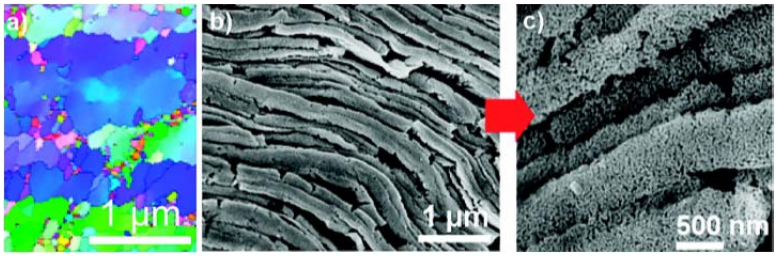

Figure 10. a) EBSD map showing the grains of a textured alloy after cold rolling. b) Low-magnification SEM image of layered structure after dealloying. c) Higher magnification SEM image showing the layered structure with embedded nanoporosity. Adapted with permission from ref.[122] Copyright 2012 American Chemical Society.

3.2.1. Film Deposition on np Ligaments

The challenge of material deposition onto the ligaments of np metals is to achieve uniform coatings on these ultrahigh aspect ratio materials (where aspect ratio is defined as the ratio between the pore length and the pore diameter). This is specifically true for bulk np metals regardless if they have nonhierarchical or hierarchical porosities. Deposition requires mass transport of some sort (for example via ion diffusion in electrodeposition) through the porous network. Concurrent deposition leads to depletion of the species to be deposited, which results in inhomogeneous coatings. Achieving truly homogeneous coatings in bulk np materials thus requires a deposition technique that is self-limiting, that is, after deposition of a certain amount of material the surface becomes passivated against further deposition. One technique that fulfills this requirement is atomic layer deposition (ALD), a chemical vapor deposition process that relies on two sequential, self-limiting surface reactions. The technique has been successfully used to deposit extremely thin (as thin as 0.25nm per cycle) and conformal layers of both metals and metal oxides on np bulk materials.[123] The layer thickness is controlled by the number of ALD cycles. Biener et al.[123] used this technique to coat np-Au samples with either Al2O2, chosen for its thermal stability, or TiO2, targeted for catalytic properties. Liquid impregnation with a metal salt solution followed by freeze drying and reduction has also been successfully applied to uniformly deposit sub-monolayer amounts of Ni on the ligaments of bulk np-Cu.[124] Here, the amount of deposited metal/metal oxide is controlled by the metal salt concentration of the solution used for impregnation; freeze drying then preserves the uniformity of the metal ion distribution during drying.[124] Air drying of the impregnated sample has also been used for applications where the uniformity of the deposited material is not a critical issue. Electroless deposition, underpotential deposition (upd), and galvanic exchange/replacement are other frequently used techniques to deposit metals or metal oxides on np metals. However, all of these techniques have limitations with respect to the sample thickness

that can still be uniformly coated (typically 100nm up to a few microns). The underlying causes of this limitation include mass transport limitations (electroless deposition), voltage drop across the sample (upd), and nonlocal reactions (galvanic exchange/replacement). To overcome the diffusion limitation of conventional electroless plating that results in non-uniform coatings with the interior of the sample uncoated, Ding et al.[125] developed a gas-liquid interphase electroless plating technique to uniformly coat np-Au leaf with Pt. The same gas-liquid (N_2H_4–$KMnO_4$) interphase electroless plating technique was later used by Lang et al.[126] to fabricate a np-Au leaf/MnO_2 composite material. This is an interesting electrode material for electrochemical supercapacitors as it combines the high electrical conductivity on np-Au with the high charge storage capacitance of MnO_2. The material and its performance will be discussed in more detail in Section 4, which is dedicated to functional properties and applications. In another example, upd was used to deposit an ultra-thin and conformal Cu layer onto the np-Au wire arrays discussed in Section 3.2.1.[88,127] The Cu coated arrays are subsequently submerged in an aqueous solution containing Pt ions where the Cu is replaced by Pt in a spontaneous displacement reaction, resulting in a Au/Pt bimetallic material.[128] The same technique was used for Pt deposition on bulk np-Au.[129] Thicker coatings can be achieved by repeating the upd and ion displacement reaction process, as demonstrated for the deposition of Pd on np-Au.[130–132] Displacement reactions of Cu with Au and Pd/Pt, respectively,have alsobeen exploitedtodecoratenp-Cu withAuor Pt metals to generate inexpensive, core-shell nanostructures.[133,134] Finally, polymer/np-Au leaf composites have been fabricated by electrochemical oxidative polymerization of aniline in 0.5M sulfuric acid.[135,136] The resulting polyaniline (PANI) layer shows excellent coverage and uniformity, and can be grown up to a thickness of 5–10nm (Figure 11). The PANI /np-Au composite is an interestingmaterial for electrical energy storage as it combines the high conductivity of np-Au (high power density) with the high electrical charge capacitance of PANI (high energy density).[135]

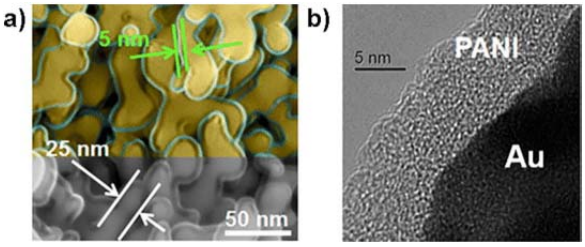

Figure 11. Left; color enhanced SEM image of PANI coated np-Au. Right; TEM image of PANI layer on the surface of np-Au. Reprinted from ref.[136] with the permission of AIP Publishing.

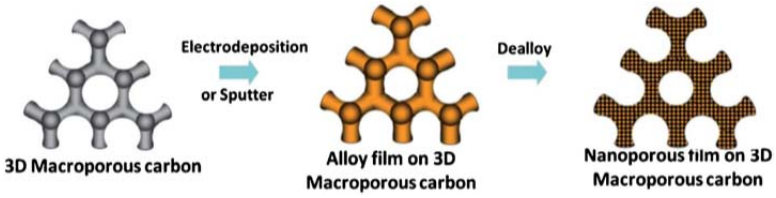

Figure 12. Schematic representation of the general process of depositing np metal films onto cellular structures. First, an alloy is deposited or sputtered onto a porous template. The alloy is then dealloyed so that the remaining material is a macroporous foam with a nanoporous coating. Reproduced from ref.[137] with permission of The Royal Society of Chemistry.

3.2.2. Nanoporous Metals as Coatings

In contrast to composite materials where np metal ligaments have been coated by supplemental elements, this section discusses np metals being used as a coating on preexisting porous structures. A schematic representation for one way to generate this type of material is shown in Figure 12: A template is coated by an alloy film, which is then dealloyed to remove the less noble element and reveal a np coating. Hierarchical np-Au–C or Ag–C composite structures have been produced in this manner, where Au–Ag or Al–Ag binary alloys are placed on macroporous carbon (Figure 13a).[137] After coating by sputtering or electrodeposition, the film is dealloyed to generate the np film shown in Figure 13b. The

multimodal porosity is described by a pore diameter of about 800 nm, from the coated carbon, and the np film ligaments, which are as small as 10nm for np-Au and 70nm for np-Ag. The same principles were used to develop a bimetallic electrode of np-Au mounted on a macroporous Ni foam (Figure 13c–d), which was made by electrodepositing a Au–Sn alloy film followed by dealloying in 5M NaOH and 1M H_2O_2. The pore size of the Ni foam is between 100 and 200mm, while the nanopores are between 30 and 90 nm.[138] A follow-up study on these materials involved an additional electrodeposition step to coat the surface with Pd for enhanced H_2O_2 electroreduction.[139] Additional application-based benefits from the hierarchical structures are discussed in detail in Section 4.

4. Properties and Applications

Many promising opportunities for using np metals as functional materials exploit the large specific surface area in the pore space. Local processes at the surface of the pores or at their interface with a fluid are exploited for applications in fields such as catalysis,[11,47–50] sensing,[11,51,52] actuation (see below), optical switching,[140–142] electropumping for microfluidic devices,[143] integrated circuit contacting,[144] biological implants,[145–148] and as electrodes where a large surface area is needed.[149–151] In most instances, the function exploits the transport of mass and/or of electric signals in the form of ions through the open pore space. Non-hierarchical nanoporosity, however, restricts mass transport and thus response time.[24] It has been pointed out that many of the applications listed above therefore entail conflicting requirements on the material structure.[97,152] Function requires high surface area with many active surface sites and, hence, small pores. On the other hand, fast response to external signals requires a network of interconnected macropores that act as a "highway" system enabling fast mass transport. Structural hierarchy is the obvious approach toward reconciling these conflicting requirements. A simple hierarchical structure will contain small pores at the lower hierarchy level to achieve local function, combined with large pores at an upper hierarchy level in order to achieve fast mass transport. In the present section, we will follow our earlier theme and first explore single element materials, followed by a discussion on composite materials that exploit the symbiotic relationship of base np metals and their composite counterparts. As the key areas of functionality we identify actuation, catalysis, sensing, and applications as capacitors and battery components; see the schematic representation Figure 14. Since large surface area combined with fast mass transport are the drivers for implementing structural hierarchy, we start out with a brief inspection of this topic.

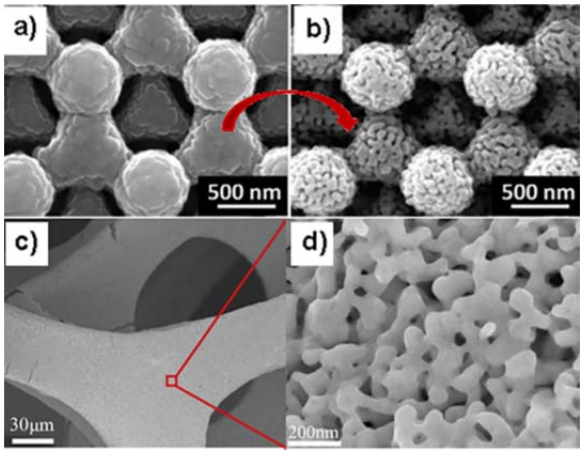

Figure 13. Examples of np metals mounted on cellular scaffolds. a and b) np Ag on porous carbon produced by sputtering of AlAg then dealloying.[137] c and d) np-Au on commercial Ni foams produced by electrodeposition of AuSn then dealloying.[138] a and b) reproduced from ref.[137] with permission of The Royal Society of Chemistry. c and d) reprinted from ref.[138] with permission from Elsevier.

4.1. Specific Surface Area and Transport Rates

Many of the reviewed applications, especially catalysis, and batteries, are dependent on a combination of large surface area and fast transport. Since the pore space in nanoporous metals is open, the concept of "electrochemically active surface area" (EASA), which is relevant to electrochemical energy storage designs, is identical to the net surface area.

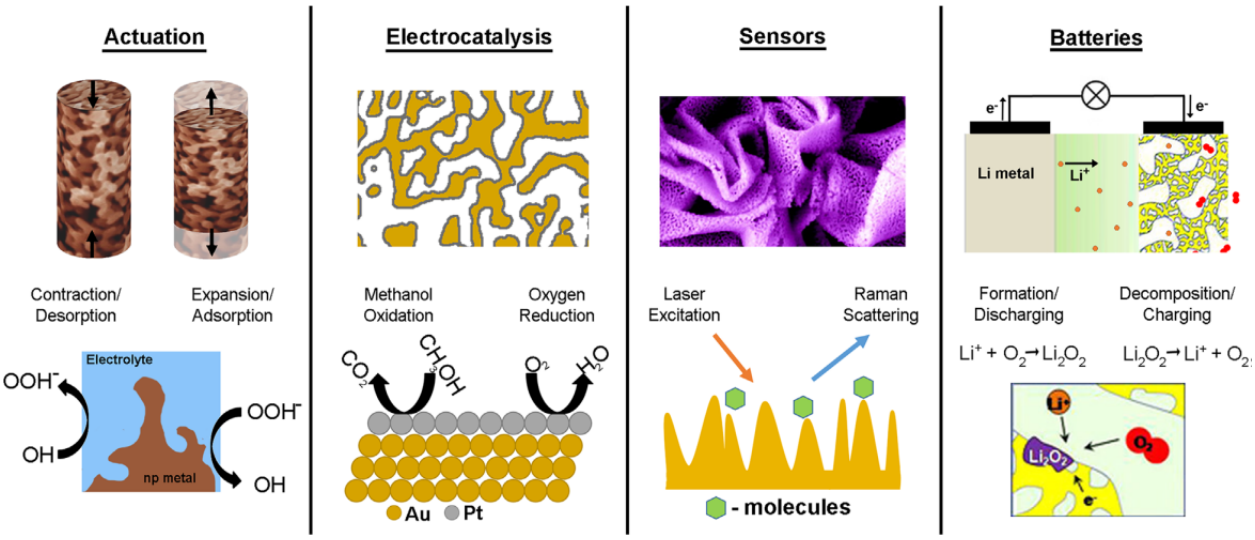

Figure 14. Schematics showing potential applications for hierarchical nanoporous materials. Actuation: np sample contraction and expansion when OH is adsorbed or desorbed from the np surface. Catalysis: electrooxidation of methanol and oxygen reduction by nanoporous metal surface. Sensors: enhanced Raman scattering of incident light from roughened np films. Top image adapted with permission from ref.[172] Copyright 2011 American Chemical Society. Batteries: hierarchical Li–O2 np electrode batteries. Adapted from ref.[201]

Table 1 lists specific surface area values for a selection of materials. Also listed are measures for the reported "peak currents," which may provide an indication of transport rates. The compilation in Table 1 prefers values from the areas of energy storage and catalysis; more values can be found in studies of porous metals linked to other areas. Many technological processes are standardized to work with the specific base solid, for instance carbon, and it is then of interest to classify materials by mass specific surface area. This parameter is also reported in many scientific publications. However, this is often impractical since mass-specific surface areas are of little meaning when the Archimedes density of the solid phase changes. By contrast, the volume-specific area of surface (per volume of the solid phase) scales inversely with characteristic structure size. Therefore, this parameter is linked to the defining microstructural length scale. It is therefore stipulated to report volume-specific surface areas as a matter of routine in scientific studies of porous materials. Table 1 also provides catalytic benchmark information, such as peak current densities, grouped by catalytic reaction for readers interested in a direct comparison of electrocatalytic performance.

4.2. Actuation and Active Strain Sensing

One of the consequences of the extremely large specific surface area of np metals is that the interior of their ligaments experiences large elastic strain. The strain originates in the stress that is required for compensating the capillary forces acting along the many surfaces.[153] As it turns out, these forces can be controlled through externally imposed electric[53,154] or chemical[155] potentials. Np metal bodies can then be made to expand or contract on demand. In other words, they can function as actuators. The surface-induced mean stress and, therefore, the macroscopic strain are linear functions of surface area per volume of the solid phase.[153] Functionalizing np metals to become electrochemical actuators uses a materials design strategy that converts the porous metal into a hybrid nanomaterial by filling the pore space with an ionic conductor, typically water. The metal–water hybrid material is distinguished by its two separate and interpenetrating conduction paths: the metal skeleton conducts electrons while the water conducts ions. Since the two pathways are capacitively coupled along the internal surface, superficial space charge layers can be set up under the control of a potential difference between the pathways. The space charge controls the interatomic bond forces in the metal and, thereby, the surface stress.[156,157] In this way reversible effective mean strains of the metal network, or relative changes of the external dimensions of nanoporous bodies, have been demonstrated in Au,[53] Ag,[158] Pd,[159] Pt,[154] with strain amplitudes reaching up to 0.65%.[76] The macroscopic strain of the network is isotropic, so that 0.65% linear strain imply 2.0% reversible volume change. In a phenomenological description of electrochemical npmetal actuators, the stresses and strains can

Table 1. Voltammetry parameters for methanol and ethanol oxidation on hierarchical nanoporous materials. Key parameters include the electrochemically active surface area (EASA) and the forward peak current density. The ratio between the forward and reverse peak current densities, which indicates tolerance to poisonous species, is also presented. Note that the data is grouped by reference.

Reaction	Material	EASA [$m^2 g^{-1}$]	Sweep Rate [$mV s^{-1}$]	Onset Potential [V]	f-Peak Current Density [$mA\ cm^{-2}$]	j-f/j-b	Source
Methanol	np-Pd rods	20.5[a]	50	−0.401	223.52[d]	1.53[b]	[111]
	np-Au	–	10	−0.5 V	0.0884	–	[189]
	np-Au w/Pt coating	–	10	−0.7 V	0.14[b]	1.55[b]	"
	np-Au w/porous Pt coating	48.3[c]	50	–	0.65[b]	1.44[b]	[190]
	np-Au w/porous Pt coating	67.04[c]	50	–	0.68[b]	1.42[b]	"
	np-Au w/porous Pt coating	70.4 (264.07[c])	50	–	1.1[b]	1.1[b]	"
	Pt-plate		50	–	0.15[b]	1[b]	"
	Tubular Mesoporous Pt/Cu	32.4	20	–	2.49[b]	1.55	[134]
	Commercial Pt Catalyst	–	20	–	0.7[b]	0.81	"
	np-Au w/Pt coating	150	10	–	650[b,d]	2.3	[195]
	Pt-Ru	–	10	–	450[b,d]	1.1	"
	np-Cu w/Au coating	–	20	−0.05	18.9[e]	–	[133]
	np-PtNi nanowire	40.4	50	–	5.31	0.8[b]	[197]
	np-PtCo nanowire	31.1	50	–	5.43	0.9[b]	"
	Pt/C E-TEK	36.5	50	–	1.36	0.78[b]	"
	PtRu/C E-TEK	13.3	50	–	3.77	1.15[b]	"
	np-PtCo nanowire	37.6	50	–	2.38	0.90	[88]
	np-PtCo nanowire	46.4	50	–	5.57	0.88	"
	Pt/C 30 E-TEK	53.3	50	–	1.26	0.76	"
	PtCo/C E-TEK	48.7	50	–	1.70	1.32	"
	Hierarchical np-Au-Cu	–	20	−0.08	25	–	[216]
	Hierarchical np-PdAl	8.9[a]	10	−0.307	53.41	1.57[b]	[49]
	Hierarchical np-PdAl	10.8[a]	10	−0.366	105.16	1.17[b]	"
	Pt decorated np-Au	10.6	50	–	1.21	1.23	[217]
	Pt/C Catalyst	–	50	–	0.95	0.77	"
Ethanol	Hierarchical np-Pd	70	50	−0.552[e]	221.2	1.27	[90]
	Hierarchical np-Pd	50.47	50	−0.519[e]	255.1	1.37	"
	Pd plate		50	−0.37[e]	–	–	"
	Hierarchical np-PdAl	8.9[a]	10	−0.461	52.66	0.72[b]	[49]
	Hierarchical np-PdAl	10.8[a]	10	−0.501	90.64	0.71[b]	"
	Hierarchical np-AgPd alloy	30.74 cm^{-2}	50	–	1.17	3.74	[134]
	np-Pd	25.56 cm^{-2}	50	–	0.65	0.99	"

[a] Determined by CO stripping method.
[b] Values approximated from figures in the corresponding reference.
[c] Units are in $m^2 cm^{-3}$.
[d] Units are in $mA mg^{-1}$.
[e] Units are in mV.

be derived from free energy functions that include the superficial charge density at pore surfaces as a state variable.[160] AMaxwell relation relates the local surface-stresscharge coupling tothe response of the local electrode potential to strain[161] and has been precisely verified in experiments.[162] The relation implies that the same phenomena that give rise to the actuation behavior can be exploited for inverting the operation principle; np metals can afford active strain sensing because they react to external loads by generating electric signals. Stenner et al.[52] have shown that the sensing and actuation behavior of np-Au are quantitatively consistent with a common thermodynamic framework. This implies that a gold-water hybrid nanomaterial effectively exhibits piezoelectric behavior.[52] Because of the many active sites at internal

surfaces, the chargeload response of np-Au is unusually robust. The electrical modification of the stress state at the surface may be amplified when pseudo-capacitive processes are incorporated. This has been demonstrated for Ni (Figure 15b), where surface layers of nickel hydroxide, several molecules in thickness, can undergo cycles of the oxidation state.[102,163] Strain amplitudes up to 2% have been achieved in this way.[102] The strain amplitude may be amplified in microstructures with multiple length-scales. Maximum strain amplitudes of up to 6% have been reported for layer structures of np-Au in which loosely connected layers buckle and thereby achieve large displacements in the direction of their normal.[122] Thin films of nanoporous metal can actuate with switching times well below one second.[164] Yet, the switching time for actuation with larger nanoporous metal bodies is limited by the time required for the electrical migration of ions into the pore space. This is another instance where hierarchical structuring may be beneficial, since small pores at the lower hierarchy level may afford the required large specific surface area while larger pores at an upper hierarchy level may accelerate the transport. Examples for the above strategy have recently been provided by studies of actuation with np-Pd.[71,165,166] These studies highlight yet another opportunity by demonstrating that the actuation strain can be enhanced by exploiting the reversible absorption of interstitials into the bulk of the ligaments rather than capacitive or pseudo-capacitive processes at their surface. The samples of refs.[52,162] inherited their multiscale structure from the multiphase microstructure of the master alloy, as generated during solidification. Nanoporous metal made in this way typically exhibits an abundance of native cracks at the scale (microns) of the features from solidification. The cracks imply brittleness even in compression, raising the question if the material has the loadbearing capability that is required for actuation. Shi et al.[71] have shown that dealloying single-phase solid solutions of Cu-Pd may lead to hierarchical np-Pd with a uniform microstructure, somewhat similar to the nestednetwork structure of ref.[152] This material is highly deformable in compression without failure. It exhibits hydrogen-enhanced actuation with amplitudes up to 4%, stable actuation over >1000 cycles and switching times of 10 s of seconds. Systematic studies of the impact of structural hierarchy on actuation, specifically on the rate of switching, or on active strain sensing remain to be reported.

4.3. Surface-Enhanced Raman Scattering

Np metals are excellent substrates for surface enhanced Raman scattering (SERS) sensing of low concentration analytes due to nanoscale roughness and gaps on the surface from nanoporosity.

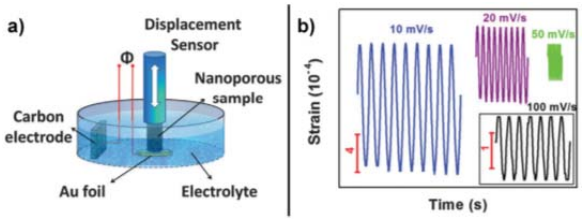

Figure 15. a) Schematic of the model actuator and a displacement sensor for strain amplitude measurement. b) Reversible strain amplitudes of the np-Ni sample during CV cycling for different scan rates. Reproduced from ref.[102] with permission of The Royal Society of Chemistry.

Gold, silver, and copper, which can all be synthesized in np morphologies, are typically used for SERS-based sensing, which detects amplified Raman signals from active analyte molecules that have been adsorbed onto metal surfaces.[167] Furthermore, several groups have demonstrated that various SERS enhancement factors can be achieved by tuning the pore size of np- Au.[168–170] More recent efforts have aimed to increase SERS response by incorporating supplemental surface features. For example, Qian et al.[171] decorated np-Au with Au nanoparticles by infiltrating the nanopores. The addition of the nanoparticles significantly enhanced the Raman scattering when compared to np-Au. Zhang et al.[172] also demonstrated improved Raman scattering for wrinkled np-Au films, which are produced by the thermal shrinkage of the film substrate. A hundred-fold increase in the SERS enhancement was observed for the wrinkled np-Au films when compared to flat np films. A hierarchical porous gold structure with aligned arrays of _100nm holes and evenly distributed mesopores also exhibited superior SERS activities compared to commercial materials, see Figure 16.[173] In addition to np-Au, np-Cu has also been investigated for SERS applications. Most notably, Chen et al.[174] showed that the

SERS response of nanostructured Cu could be tailored by altering ligament sizes. At the optimum pore size, np-Cu achieved SERS enhancement factors (_1.85_10_5) that are comparable to np-Au. Although not extensively studied, other hierarchical np materials have also been developed for alternative sensing applications. One such study used np-Au nanowires for sensing the adsorption of octadecanthiol, which resulted in detection sensitivities comparable to ultrathin films.[84] Np–Au films mounted on commercial Ni foams were shown to detect hydrazine gas and hydrogen peroxide.[175] Finally, bimodal np-Pt–Ti have been explored for the sensing of ascorbic acid, dopamine, and uric acid.[176]

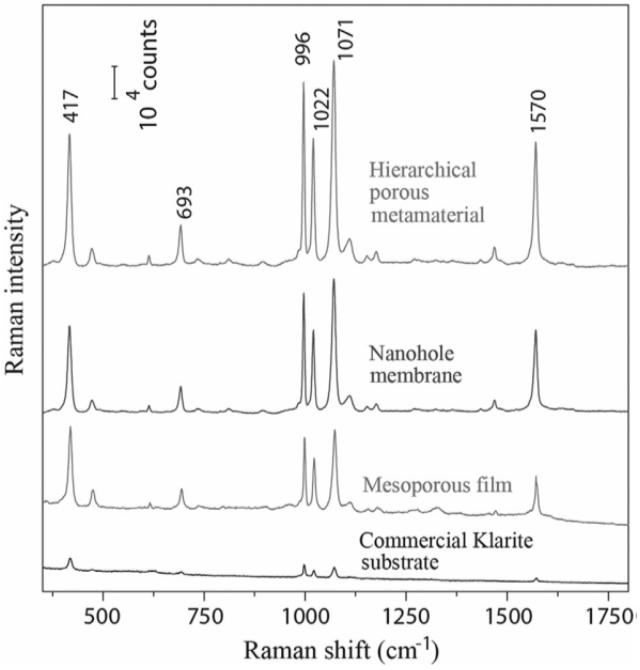

Figure 16. SERS spectra on (from bottom to top) a commercial Klarite substrate, mesoporous film, nanohole membrane, and a hierarchical structure with a nanohole membrane and mesoporous film. Adapted with permission from ref.[173] Copyright 2014 John Wiley and Sons.

4.4. Catalytic Applications

To date, the most studied and viable application of np metals is catalysis. Raney nickel, first developed in 1926, is used for a variety of industrially important hydrogenation reactions, and Raney copper is a widely-used catalyst for the water-gas shift reaction.[177] Recent advancements in synthetic methods, paired with high electrical conductivity, high surface area, and a high density of reactive sites make np metals highly efficient heterogeneous catalysts and electrocatalysts. Examples include the electrooxidation of methanol and ethanol, as well as the electroreduction of oxygen, carbon monoxide, and carbon dioxide. For fuel cell applications, Pt remains to be the preferred catalyst material despite its high cost due to its superior catalytic activity. By contrast, the production and conversion of many important platform chemicals requires more selective and thus less reactive metals than Pt. Here, recent developments in the field of noble metal based dilute alloy np catalysts have been very promising.[178] The idea behind this development is that the noble metal majority alloy component provides the desired selectivity while the minority alloy component provides reactive sites for critical reaction steps. It is also important to understand that the catalytic properties of these materials also strongly depend on the surface chemical composition under reaction condition. This can be very different from the surface composition present when the material was initially prepared and characterized. A good example is np-Au prepared from Ag–Au alloys, which is actually a dilute alloy bimetallic system. As recently demonstrated by in situ microscopy and spectroscopy, activation by ozone enriches the surface in Ag and leads to the formation of active sites for O2 activation.[179] For this section, np metals are discussed first, followed by a section on np composite catalysts. Keeping with the format of this review, materials are discussed by structure type but categorized by catalytic reaction in Table 1.

4.4.1. Metal Catalysts

A 2003 study revealed that np-Pt has improved methanol oxidation activity compared to polycrystalline Pt, suggesting that material architecture can play a role in promoting catalytic activity.[180] Furthermore, the same material shows reduced oxygen reduction capabilities since approximately three quarters of the internal pore surface area is inaccessible.[180] This is likely due to poor ion penetration of the sample because the small pore size obstructs fluid flow.[12] Utilization of the inner surface area could be improved by a multimodal pore distribution or architecture where larger pores make the smaller pores more accessible for ions.

Hierarchical np-Pd, synthesized by dealloying of Pd–Al alloys with multiple phases, is also an effective catalyst for alcohol oxidation.[96,181] In the former study, nested bimodal np-Pd exhibited improved reaction kinetics for ethanol oxidation when compared to a Pd plate electrode and nonhierarchical np-Pd.[96] In the same study, two bimodal structures, one with larger pores than the other, were compared for catalytic activity. Interestingly, the nested structure with larger pore sizes, but with lower surface area, showed a higher reactivity for ethanol oxidation.

Aside from bimodal single element catalysts, bimodal np alloys have also shown intriguing catalytic activity for several desirable reactions. Compared to np-Pt and commercial Pt/C catalysts, hierarchical np-Pt–Fe retains more EASA after 5000 cycles and also shows significantly decreased CO poisoning during methanol oxidation.[111] Np–Pt–Au is another example of an alloy that has shown superior catalytic activity, particularly for formic acid oxidation, with higher current densities in both forward and reverse voltage scans when compared to Pt/C.[182] Oxygen reduction was studied on bimodal Pt–Al intermetallics with an atomic layer of Pt at the surface. The specific activity was about five times higher than that of Pt/C catalysts.[183] Finally, ethanol oxidation was explored using bimodal np-Ag–Pd alloys. Although not compared against a commercial catalyst, np-Ag–Pd showed a higher ratio of anodic peaks, indicating better poisoning tolerance, and a lower peak potential, indicating more favorable ethanol oxidation, than np-Pd.[184]

Nanoporous nanoparticles, which are inherently hierarchical, have also been studied for their catalytic properties since they have a higher surface-to-volume ratio than bulk np metals or nanoparticles.[185] In one study, np-Pt–Cu and np-Pt–Co nanoparticles were investigated for their particle size dependent np morphology and catalytic activity for oxygen reduction.[186] It was found that both types of alloy np nanoparticles showed enhanced surface activity compared to a commercial Pt/C catalyst. A study on np-Pt–Ni nanoparticles, yielded similar results, where the mass specific activity for oxygen reduction was about four times higher than the compared commercial catalyst.[187] A separate investigation of np-Pt–Ni nanoparticles showed that the EASA of the np particle is about 2.5 times greater than that of Pt–Ni nanoparticles.[188] While the increase in EASA surface area of nanoparticles is advantageous, several other factors influencing the catalytic activity must be addressed, including particle size distribution, particle agglomeration, and the choice of particle dispersion support.

Previously, pure Au has shown catalytic activity in the form of supported nanoparticles (<5 nm), but several studies found that larger np-Au samples with ligaments between 12 and 30nm can be effective catalysts for both methanol and CO oxidation,[50,189,190] as well as oxygen and hydrogen peroxide reduction.[48,191] Reproducible catalyst activation of these np- Au catalysts is critical but can be achieved through an ozone treatment at atmospheric pressure.[192] Similar to the previously mentioned np-Pt, there are mass transport limitations due to the tortuous porosity of the material, which become more severe with decreasing pore size.[24] The importance of the material architecture is illustrated by the results of a recent study that evaluated the reactivity of np-Au catalysts in three different forms: ingots, foils, and hollow shells.[192] The study revealed that the conversion rates of methanol to methylformate are five times higher for the hollow shell and foil morphology when compared to the ingot.[192] The higher conversion rates for foils and porous shells reveal that these morphologies can mitigate the mass transport limitations that are inherent to non-hierarchical bulk np materials. As pointed out before, hierarchical pore morphologies are ideally suited for applications such as catalysis that benefit from the combination of high surface area (provided by nanopores) and fast mass transport (provided by macropores). Further insight into mass transport for catalysis in

nanoporous materials is given in a study by Snyder et al.,[193] where quantitative measurements of EASA are given as a function of both overpotential and the dealloyed volume of similarly sized np-NiPt samples. It was found that for samples with a larger dealloyed volume or roughness factor (i.e., longer dealloying times), the EASA increases with decreasing overpotential. This is related to the diffusion of oxygen molecules into the porous structure, where the molecules will diffuse further into the np network at lower overpotentials, but will reduce at the exterior surfaces at high overpotentials.[193] Therefore, the active surface area during oxygen reduction is a balance between the applied overpotential and the depth molecules must travel to utilize all the np ligament surfaces.

4.4.2. Composite Catalysts

Coating of np metals with additional materials provides another avenue for tailoring catalytic activity and selectivity of these materials. As discussed in detail in Section 3.3.1, achieving uniform coatings on these ultrahigh aspect ratio materials remains to be very challenging, and only a few techniques are suited to generate deposits of the desired spatial uniformity. However, if successful, the coating approach can result in large performance improvements. For example, coating the ligaments of np-Au with Pt or Pd (for synthesis details, refer to Section 3.3.1)[194] creates a bimetallic np material that, if used as an electrode in fuel cells, performs as well as conventional Pt/C catalysts but with much lower Pt loading. Other work has shown that Pt coated np-Au (referred to as NPG-Pt) has enhanced structural stability with better catalytic activity for methanol reduction and resistance to catalyst poisoning from CO than commercial Pt/Ru catalysts.[195] In a similar study, the long-term formic acid oxidation stability of the bimetallic structures was improved by depositing a layer of Au clusters on top of the Pt so that areas of the Pt layer are still exposed (referred to as NPG–Pt– Au).[129] The Au clusters disrupt the continuous Pt layer and are believed to shorten the reaction path of formic acid by preventing CO poisoning. These materials also retained a significant amount of EASA, where the EASA loss of NPG–Pt–Au was 45% compared to a 75% loss for NPG–Pt.[129] An analogous study explored the methanol oxidation of np-Au coated with porous Pt deposits, which are characterized as small islands rather than a conformal layer (Figure 17a).[196] These samples exhibited activity for methanol oxidation, while bare NPG showed none (Figure 17b). Furthermore, higher Pt content increases catalytic activity from the availability of additional Pt sites.[196] Another example demonstrating the catalytic improvements that can be achieved by Pt deposition on np metal surfaces is a study by Shin et al.,[88] which showed that np tubes (Figure 5b) with a thin Pt layer exhibited better methanol reduction activity compared to smooth-walled tube arrays and carbon-supported Pt nanoparticles. This is likely due to a higher CO poisoning tolerance that has been established for these types of bimetallic materials.[88]

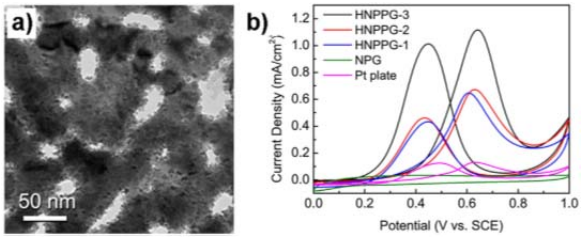

Figure 17. a) TEM image of HNPPG-2 showing non-conformal Pt islands forming a porous film. b) CV curves for methanol oxidation for a Pt plate, bare NPG and NPG coated with various amounts of porous Pt. As the Pt content increases, the current density increases. Reproduced by permission from Macmillan Publishers Ltd: Scientific Report, ref.[196] Copyright 2014.

So far we have discussed the effect of Pt coatings on the catalytic performance of np metals. Another metal that is frequently used to tailor the reactivity of np metals is Pd. For example, Kiani and Fard showed that a Pd monolayer coating, comparable to the Pt coatings discussed above, increased the oxygen reduction activity of np-Au when compared to both a bare np-Au or a flat Pd-decorated electrode.[130] In another study, the Zhang group showed that the hydrogen storage capability of Pd-coated np-Au increases with increasing number of monolayer Pd deposition cycles, suggesting potential applications as an electrocatalyst.[132] More recent work specifically investigated the electocatalytic activity for oxygen reduction, and revealed that Pd coated np-Au shows a higher oxygen reduction activity than np-Au or a commercial Pt/C catalyst. The highest

specific oxygen reduction activity was found when only a single layer of Pd was deposited on the np-Au surface.[131]

Another potential substrate for thin layer depositions is np- Cu, which is economical, highly conductive, and easily coated with Au via a spontaneous replacement reaction. Chen et al.[133] showed that a Au on np-Cu composite (Au np- Cu) exhibits significant electrocatalytic activity for the oxidation of methanol as judged by both higher peak current and lower onset potential for methanol oxidation as compared to np-Au. That material also showed good electrochemical stability, retaining over 90% of its activity after 100 cycles compared to 57% for np-Au. It is important to note that even very small loading levels can dramatically affect the reactivity of np-metals. For example, it has recently been shown that deposition of as little as 0.3 at% Ni on np-Cu dramatically lowers the activation barrier for selective dehydrogenation of ethanol to acetaldehyde, from _70 kJ mol_1 for np-Cu to _45 kJ mol_1 for np-Ni0.003Cu.[124]

Nanowire arrays generated from a variety of np metals have also been studied as catalytic supports because such structures combine an open morphology to facilitate fluid flow and high surface area for activity. For example, mesoporous nanotubular Pt–Cu alloys (Figure 18a) have three times higher specific activity and higher CO poisoning tolerance than that of commercial Pt/C.[134] Several other types of alloy np nanowires have been generated through mild or incomplete dealloying by Liu et al.,[89,197,198] including np-Pt–Co, Pt–Ni, Pt–Co–Ni, Pt–Co– Au, and Pt–Ru–Co–Ni. These nanowires showed enhanced catalytic activity for methanol oxidation when compared to commercially available catalysts. In addition to catalytic activity, the ternary (and quaternary) alloy nanowires were investigated for durability, where the Pt–Ru–Co–Ni nanowires retained over 90% of their active surface area after 1000 cycles. For further comparison, the np-Pt–Ni nanowires shown in Figure 18b and c exhibited higher activity than Pt–Co with similar Pt content. Other np

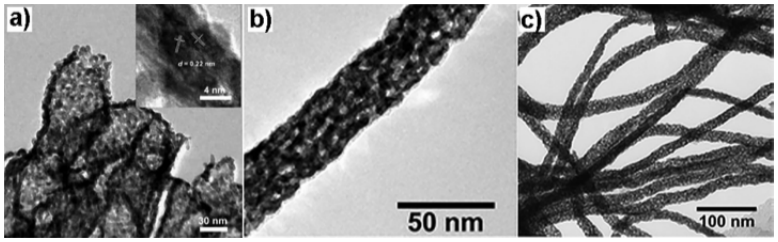

wires synthesized by mild dealloying include interwoven Pt–Fe nanowires, which also demonstrate better oxygen reduction and durability than Pt/C.[199]

Figure 18. a) Mesoporous nanotubular PtCu structures with core-shell shapes.[134] b) Single PtNi nanoporous nanowire showing pore sizes below 5 nm.[197] c) bundle of np-PtNi nanowires.[197] a) adapted with permission from.[134] Copyright 2009 John Wiley and Sons. b and c) reproduced from ref.[197] with permission of The Royal Society of Chemistry.

Up to this point only np metallic catalytic structures have been discussed, however np metal–metal oxide composites have also shown promise as future catalytic materials. The use of TiO2 to functionalize the surface of np-Au has also been explored. Jia et al.[200] used np-Au decorated with TiO2 nanoparticles to develop a photocatalytic electrode for methanol oxidation. In a later study, Biener et al.[123] demonstrated that highly dispersed TiO2 particles on np-Au improve the thermal and morphological stability of the metal, which has a tendency to coarsen, and also increases CO oxidation activity by 300%. The presence of TiO2 nanocrystals on the surface of np-Au increases the efficiency for O2 dissociation, which is the rate limiting step for CO oxidation with gold based catalysts, and stabilizes the high surface area of np-Au.[123]

In the synthesis section, emphasis was placed on the multimodal structures fabricated from dealloying multiphase or multi-element alloys in two-step dealloying processes. These types of materials were also investigated for their catalytic activity. Unlike the coated np materials, these hierarchical structures provide large pores for unobstructed transport of molecules and smaller pores for increased surface area and a high density of reactive sites.[108] Similar to the majority of materials discussed in this section, bimodal np structures with Pt and Pd content were studied, including hierarchical np-PtTi alloys. Compared to commercial Pt/C catalysts and similar np-Pt samples, hierarchical np-PtTi showed 3 and 2.5 times higher

mass activity for oxygen reduction, respectively. Additionally, the hierarchical structure was stable, without significant feature changes, and also showed less current degradation over time, signaling higher retention of active site availability.[108]

Hierarchical Pd–Al structures were studied for methanol and ethanol reduction, and showed enhanced activity when compared to a flat Pd electrode.[49] While no comparison was made to a commercial catalyst, the key feature of this study is the comparison between similar hierarchical structures with different feature sizes. Compared to a structure with smaller pores, the more open structure with larger pores (15–25nm vs. 3–6 nm) has a higher electrochemically active surface area. This suggests that a smaller pore size, and therefore higher geometrical surface area, may not lead to increased activity since mass transport will be more difficult with finer pore channels.[49]

General trends from this section show that Pt group metals are still relied on for catalytic function, however increased surfaced area and surface access can reduce the Pt loading necessary for high catalytic activity. Additionally, np metal materials provide structurally stable catalysts that resist agglomeration of nanoparticles and CO poisoning more effectively than commercially available catalysts. However, viable np catalysts, like those discussed here, have yet to become commercially available.

4.5. Energy Applications

4.5.1. Lithium Ion Battery Systems

Hierarchical np metals have been explored for rechargeable energy storage devices such as supercapacitors and electrodes for new battery technologies. Similar to the electrocatalysis application discussed above, these applications also benefit from the high electrical conductivity of np metals in general and the large electrochemically active surface area of hierarchical np metals in particular. Both are necessary for energy storage and fast electron/ion transport, making np metals worthwhile materials to investigate for these applications. Recently, Guo et al.[201] developed a hierarchical np-Au electrode for use in a Li–O2 battery system. Compared to non-hierarchical as-prepared np metals, the hierarchical structure increased the reversible capacity and lead to longer cycling lifetimes at low overpotentials. The high reversible capacity of about 1000mAg^{-1} is only reached for low overpotentials, however with a redox mediator, the capacity and cyclic retention are improved.

Composite materials have been successfully used to improve battery performance, such as Goodenough's layered electrodes, which were used in commercial batteries.[202] A np-Au–Sn composite electrodemade by the electroless deposition of Sn on np-Au leaf was investigated as an anode for rechargeable lithium ion batteries, and was shown to effectively accommodate the volume changes that occur during charge cycling.[203] The electrode achieves a reversible capacity of 515mAh g^{-1} in a voltage window of 0.005–1.0 V, and has a charge capacity retention of about 90% after 100 charge-discharge cycles. Sn-coated bimodal np-Cu films have also shown high charge capacity retention (95%) when cycled between 0.01 and 1.5 V.[204] However, this is only achieved after the first 10–15 charge-discharge cycles, when the initial reversible capacity has already been reduced by half. The facile plating of Sn, along with its high electronic conductivity and large capacity for storage, make it an ideal element for bimetallic anodes.

Nanoporous Cu with oxide coatings have also been investigated as Li-ion battery anodes. In one study, np-Cu/ MnO2 electrodes were integrated with a solid Cu film to form anodes with a stable reversible capacity of _1100mAhg_1 for 100 cycles. This was accomplished at a current density of 8.4Ag^{-1} after initial cycling at half that current density.[205] Other np-Cu anodes with a cuprous oxide surface demonstrated a high reversible capacity of 1.45mAhcm^{-2} after 120 cycles, where the initial capacity was 2.35mAhcm^{-2}.[151] Unlike the other anodes discussed in this section, these anodes are not freestanding films. Instead, the np-Cu is mixed in slurries and used as a coating on Ni foams.

Another noteworthy composite material is TiO2-coated np-Au, previously discussed for its electrocatalytic properties. This particular material is also an effective electrode due to the symbiotic relationship between the Au scaffold, which is a current collector, and the TiO2 coating, which acts to stabilize the structure and

store Li.[206] Theoretically, this type of structure can be fabricated from any np scaffold, such as Cu or Ni, to make the composite more economical. By providing the opportunity to independently vary both pore size and TiO2 layer thickness, the porous electrode can be optimized for Li ion diffusivity for a given electrode thickness.[206]

4.5.2. Supercapacitors

Supercapacitors can be classified as either electric double layer capacitors (EDLC), which store charge electrostatically (non- Faradaic) by polarization of the electrode–electrolyte interface, orpseudocapacitors, which store charge Faradaically (Electrode processes in which the charge can be recovered while chemical bonding or oxidation states change are properly termed "pseudocapacitive." The same processes are often also termed "Faradaic," yet that term applies equally to processes where the charge cannot be recovered, such as electrocatalytic reactions.) by involving surface redox reactions.[207] Assuming constant density, the volumetric capacitance (Fcm^{-3}) of an EDLC increases with increasing surface area of the electrode material (see Table 1). The combination of high surface area and high conductivity thus makes np metals viable materials as supercapacitors. Lang et al.[208] developed a supercapacitor device based on np-Au and tested it in both ionic liquid and alkaline solutions. With decreasing discharge current density, the volumetric capacitance increased from 9.6 to 21.6 Fcm^{-3} in the ionic liquid and from 17.1 to 24 Fcm^{-3} in an alkaline solution. The energy densities of the devices were found to be between 16.5 and 21.7mWh cm^{-3} in the ionic liquid and 4.89–8.31mWhcm_3 in KOH. For comparison, novel graphene/hydrogel capacitors have achieved an exceptionally high energy density of 60mWhcm^{-3},[209] whereas commercially available supercapacitors have an approximate energy density of 5–8mWhcm^{-3}.[210] Bimodal np-Ni alloys were also studied for their capacitive properties. A comparison of the specific areal capacitance, which was calculated from discharge curves and the electrode sheet area, at different current densities (1.25 vs. 20mAcm^{-2}) showed similar values (_1.05 vs. 1.11 Fcm^{-2}). The volumetric capacitance was also evaluated and determined to be 317 F cm^{-3} in 1M KOH.[94] This value is large in comparison to those achieved by np-Au in the previous example. However, it should be noted that the redox reactions in nickel–hydroxide layers bring a very high capacitance at Ni surfaces. Therefore, the higher capacitance of nanoporous Ni structures are likely not the result of their hierarchical structure. A direct comparison between np-Ni and bimodal np-Ni would be necessary to ascertain the influence of hierarchy on capacitance.

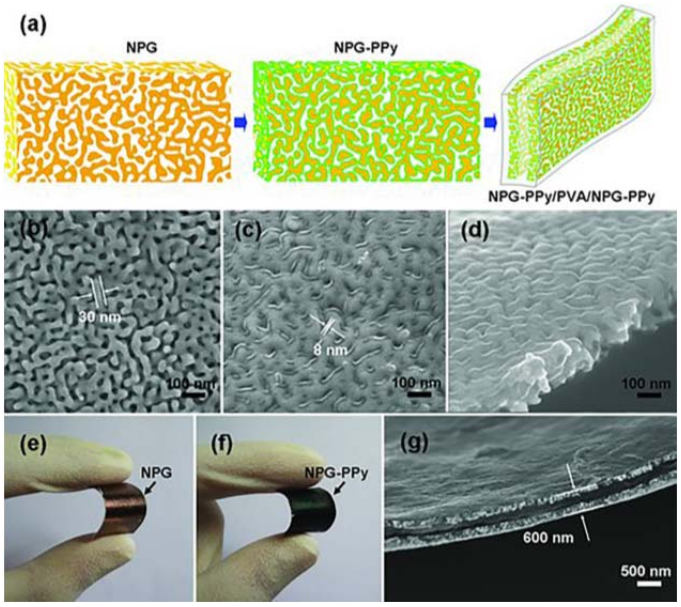

Figure 19. a) Schematic of the fabrication for polypyrrole coated np-Au. b–d) SEM images of bare and coated np-Au. e and f) Optical images of bare and coated np-Au membranes. g) SEM image of assembled supercapacitor device. Reproduced with permission from ref.[211] Copyright 2011 John Wiley and Sons.

Additionally, the coating of npmetals withmaterials that exhibit high pseudocapacitance, such as transition metal oxides and conductive polymers, could provide symbiotic material relationships. The pseudocapacitive coating can efficiently store charge by undergoing fast surface redox reactions; the low conductivity of thematerial is overcome by supporting it on high conductivity np metals, which also act as double layer capacitors. Two studies by Lang et al.[126,135] have capitalized on this design principle by coating np-Au with thin MnO2 and polyaniline films.[126,135] In the first study, the reaction kinetics of the poorly conductive metal oxide are mitigated by the conductive gold substrate, resulting in a high specific capacitance of 1145 Fg^{-1} for theMnO2 and 601 Fg^{-1} for the combined Au/MnO2 material. When used as electrodes in a supercapacitor, the metal/oxide composite material reaches an energy density of57Wh kg^{-1} and a power density of 16kWkg^{-1}.[126] In a subsequent study, polyaniline (PANI), a conductive polymer, was used as a pseudocapacitive shell on np-Au. Np–Au/PANI based supercapacitors exhibited a volumetric capacitance of 1500 Fcm_3, an energy density of 78mWhcm^{-3}, and a power density of 190Wcm^{-3}.[135] Similarly, Meng and Ding developed a supercapacitor electrode by coating np-Au with a polypyrrole (PPy) film.[211] A schematic representation of the fabrication process is shown in Figure 19a, along with SEM images of the bare (Figure 19b) and coated (Figure 19c) np-Au. The solid gel electrolyte used in this study also improved the flexibility of the np-Au electrode (Figure 19g). The evaluated capacitance reaches a maximum of 270 Fg^{-1} (per PPy mass) at a current density of 0.6Ag^{-1}. The volumetric power and energy of the entire supercapacitor device is estimated to be 56.7Wcm^{-3} and 2.8mWhcm^{-3}, respectively, while for a single electrode these values are much higher (283Wcm^{-3} and 19mWhcm^{-3}).[211] When considering the entire device, the performance of the PPy coated np-Au has substantially lower power and energy densities. An asymmetric supercapacitor was developed using two of the previously discussed electrode films; np-Au with a PPy film as the negative electrode and np-Au with MnO2 as the positive electrode.[212] These films can be used in combination due to their similar specific capacitances and overlapping voltage operation windows. The energy and power densities of the assembly were reported as 86Wh kg^{-1} and 25Wh kg^{-1}, respectively, with a device capacitance of 193 Fg^{-1}. The capacitance compared to a PPy/PPy capacitor is enhanced, but this value is reduced compared to a MnO2/MnO2 capacitor. Furthermore, the influence of the core np-Au is excluded since its specific capacitance is less than 1% of the composite films.[212] While the reported energy densities for these devices are several times higher than those reported for uncoated np-Au and possibly several orders of magnitude higher than commercial capacitors, these devices have a critical issue. The overall electrode volume, which ultimately determines the device storage capacity, is restricted by processing limitations requiring the electrodes to be thin (~100 nm).

5. Conclusions and Future Outlook

In this review, several synthesis strategies for the development of np materials with structural hierarchy have been presented. These include templating and dealloying methods, as well as multistep approaches that combine more than one processing technique. Strategies have also been demonstrated for a wide range of metals such as Au and more economical materials like Cu or Ni. In particular, hierarchical porosities can be realized by selecting suitable multi-element precursor alloys, alloy compositions, and multi-step dealloying protocols. For example, the sequential removal of different LNEs from a multi-element precursor alloy in combination with heat treatments can generate bimodal porosity. We also discussed examples for fabricating hierarchical np metal structures from binary alloys by using multiphase starting alloys (Cu–Al system) or by using alloy compositions that allow for sequential dealloying (Ag–Au system). Materials with multimodal porosity are intriguing because they help to overcome mass transport limitations in small pore networks by supporting fast transport through their macroporous system while providing the high surface area desired for catalysis through their nanoscale porosity. In particular, noble metal based materials, like np-Au and np-Pt, have been extensively explored as electrochemical catalysts because they exhibit high catalytic activity toward methanol and ethanol oxidation as well as oxygen reduction. Additionally, the fabrication of hierarchical composites, where the hierarchy comes from the spatial distribution of the elements, were also included. Synthesis methods for these hierarchical composite materials include coating of np metal surfaces with films composed of metal oxides, polymers, or other metals to enhance their chemical, thermal, and mechanical properties. Np metals can also act as functional coatings on other porous materials by depositing precursor alloys on macroporous foams and dealloying the film. In some instances, the symbiotic properties

of two base materials make hierarchical composite structures viable for energy storage applications, including electrodes for Li batteries, or supercapacitors. It is important to note that the area-specific capacitance is an electrode material/electrolyte characteristic number and is independent of the microstructure of a porous material. Thus, the energy density of a supercapacitor with hierarchical structure does not change if the porosity stays the same, but the power performance will improve. The enhanced abilities of these materials for a wide variety of applications is in part due to the large surface area of np metals and their conductivity. The addition of hierarchy and other materials has expanded the working space of np metals by improving their specific properties. Much progress has been made toward developing enhanced np materials through leveraging structure or symbiotic composites, and several applications are being explored. One particular area that deserves attention is the use of np structures to reduce the need of precious metals such as Pt or Pd for electrocatalysis. With the increased surface area and enhanced transport offered by hierarchical materials, cheaper materials may be able replace precious metal systems. Alternatively, alloying materials can also enhance the material properties of Pt, Pd, or Au alloys. Future studies on hierarchical materials should also explore structural size effects, optimum pore sizes, and surface area on catalytic behavior to further improve our ability to tailor superior catalytic electrodes for specific system or material requirements. In this regard, the use of additively manufactured structures as base materials would be beneficial since they have known geometry and thus more predictable mass transport properties. Additionally, stability during cycling or exposure to elevated temperatures must be addressed since as the material coarsens, it loses surface area and therefore its specific catalytic activity towards the desired reaction. In the area of supercapacitors, the reviewed studies developed promising proof of principle structures that demonstrate additional layers of carefully chosen materials can result in combined high double layer capacitance and pseudocapcitance from improved electron and ion transport. Subsequent work could involve the coating of multimodal structures and the subsequent tailoring of such structures, both in feature size and material composition, for further enhanced capacitive materials. Another intriguing approach would be to apply these designs to large scale production and supercapacitor fabrication techniques that are powder based. Finally, scaling up and streamlining synthesis procedures must be on the forefront of experimental work. While new hierarchical materials show promise toward particular applications, their usefulness in practice is linked to their size and straightforward production. This is necessary in applications such as energy storage since the capacity of a supercapacitor depends on both the specific capacitance and the volume of the device. Thus, despite their excellent performance, thin film electrodes remain compromised by their volume limitations. The potential practical applications of np metals with structural hierarchy are vast. The combination of control over the pore feature sizes and surface/interface composition may be the key to thoroughly understanding the influence of material structure and composition of materials on electrochemical behavior, which has repercussions in both catalysis and energy systems. It is the purpose of this review to consolidate recent work on hierarchical structures and guide researchers towards newer unexplored synthesis procedures that may lead to substantial insight on structure and functionality.

Acknowledgement

This work was performed under the auspices of the Air Force Office of Scientific Research grant FA9550-14-1-0352 and with the support of the National Defense Science and Engineering Graduate Fellowship. Work at LLNL was performed under the auspices of the U.S. Department of Energy by LLNL under Contract DE-AC52-07NA27344. JB acknowledges the support provided through the Integrated Mesoscale Architectures for Sustainable Catalysis (IMASC), an Energy Frontier Research Center funded by the U.S. Department of Energy (DOE), Office of Science, Basic Energy Sciences (BES), under Award number DE-SC0012573. JW acknowledges support by the German Research Foundation (DFG) through its Coordinated Research Area SFB 986 Tailor-Made Multiscale Materials Systems, subproject B2.

Conflict of Interest

Authors declare no conflict of interest.

Keywords

dealloying; hierarchical materials; nanoporous metals; structural hierarchy; templating Received: April 28, 2017 Revised: June 15, 2017
[1] P. Fratzl, R. Weinkamer, Prog. Mater. Sci. 2007, 52, 1263.

[2] R. Lakes, Nature 1993, 361, 511.

[3] U. G. K. Wegst, H. Bai, E. Saiz, A. P. Tomsia, R. O. Ritchie, Nat. Mater. 2015, 14, 23.

[4] K. Boomsma, D. Poulikakos, F. Zwick, Mech. Mater. 2003, 35, 1161.

[5] T. J. Lu, H. A. Stone, M. F. Ashby, Acta. Mater. 1998, 46, 3619.

[6] Porous Metal Filters Inc., PMF Handbook of Filtration and Metal Filter Technology, Texas 2016.

[7] Porvair Filtration Group, High Temperature Gas Filtration, Hampshire, UK 2016.

[8] B. A. Gama, T. A. Bogetti, B. K. Fink, C.-J. Yu, T. Dennis Claar, H. H. Eifert, J. W. Gillespie Jr, Compos. Struct. 2001, 52, 381.

[9] J. Banhart, Adv. Eng. Mater. 2013, 15, 82.

[10] L. Giani, G. Groppi, E. Tronconi, Ind. Eng. Chem. Res. 2005, 44, 4993.

[11] Y. Ding, M. W. Chen, MRS Bull. 2009, 34, 569.

[12] J. T. Zhang, C. M. Li, Chem. Soc. Rev. 2012, 41, 7016.

[13] A. Bhattacharya, V. V. Calmidi, R. L. Mahajan, Int. J. Heat Mass Transfer 2002, 45, 1017.

[14] T. A. Schaedler, W. B. Carter, Annu. Rev. Mater. Res. 2016, 46, 187.

[15] J. Banhart, Prog. Mater. Sci. 2001, 46, 559.

[16] T. J. Lu, L. Valdevit, A. G. Evans, Prog. Mater. Sci. 2005, 50, 789.

[17] S. Chiras, D. R. Mumm, A. G. Evans, N. Wicks, J. W. Hutchinson, K. Dharmasena, H. N. G. Wadley, S. Fichter, Int. J. Solids Struct. 2002, 39, 4093.

[18] A. G. Evans, J. W. Hutchinson, N. A. Fleck, M. F. Ashby, H. N. G. Wadley, Prog. Mater. Sci. 2001, 46, 309.

[19] L. Valdevit, A. J. Jacobsen, J. R. Greer, W. B. Carter, J. Am. Ceram. Soc. 2011, 94, 1.

[20] L. P. Lefebvre, J. Banhart, D. C. Dunand, Adv. Eng. Mater. 2008, 10, 775.

[21] N. Kranzlin, M. Niederberger, Mater. Horiz. 2015, 2, 359.

[22] L. J. Gison, Annu. Rev. Mater. Sci. 2000, 30, 191.

[23] V. S. Deshpande, M. F. Ashby, N. A. Fleck, Acta. Mater. 2001, 49, 1035.

[24] G. Falcucci, S. Succi, A. Montessori, S. Melchionna, P. Prestininzi, C. Barroo, D. C. Bell, M. M. Biener, J. Biener, B. Zugic, E. Kaxiras, Microfluid. Nanofluid. 2016, 20, 1.

[25] C. Y. Zhao, W. Lu, Y. Tian, Sol. Energy 2010, 84, 1402.

[26] A. Bhattacharya, R. L. Mahajan, J. Electron. Packag. 2002, 124, 155.

[27] L. J. Gibson, M. F. Ashby, Cellular Solids: Structure and Properties, Cambridge University Press, Cambridge 1997.

[28] A. M. Hodge, J. Biener, J. R. Hayes, P. M. Bythrow, C. A. Volkert, A. V. Hamza, Acta. Mater. 2007, 55, 1343.

[29] N. Huber, R. N. Viswanath, N. Mameka, J. Markmann, J. Weissmüller, Acta. Mater. 2014, 67, 252.

[30] B. Roschning, N. Huber, J. Mech. Phys. Solids 2016, 92, 55.

[31] J. Biener, A. V. Hamza, A. M. Hodge, in Micro and Nano Mechanical Testing of Materials and Devices, Springer, US 2008, 118.

[32] J. Weissmuller, R. C. Newman, H. J. Jin, A. M. Hodge, J. W. Kysar, MRS Bull. 2009, 34, 577.

[33] N. Mameka, K. Wang, J. Markmann, E. T. Lilleodden, J. Weissmüller, Mater. Res. Lett. 2016, 4, 27.

[34] J. Biener, A. M. Hodge, A. V. Hamza, L. M. Hsiung, J. H. Satcher Jr, J. Appl. Phys. 2005, 97, 024301.

[35] J. Biener, A. M. Hodge, J. R. Hayes, C. A. Volkert, L. A. Zepeda-Ruiz, A. V. Hamza, F. F. Abraham, Nano Lett. 2006, 6, 2379.

[36] C. Volkert, E. Lilleodden, D. Kramer, J. Weissmüller, Appl. Phys. Lett. 2006, 89, 061920.

[37] R. Li, K. Sieradzki, Phys. Rev. Lett. 1992, 68, 1168.

[38] M. Hakamada, M. Mabuchi, Scr. Mater. 2007, 56, 1003.

[39] T. J. Balk, C. Eberl, Y. Sun, K. J. Hemker, D. S. Gianola, JOM 2009, 61, 26.

[40] H. J. Jin, L. Kurmanaeva, J. Schmauch, H. Rosner, Y. Ivanisenko, J. Weissmuller, Acta. Mater. 2009, 57, 2665.

[41] H. Gao, Int. J. Fract. 2006, 138, 101.

[42] B. Ji, H. Gao, J. Mech. Phys. Solids 2004, 52, 1963.

[43] M. A. De Meller, Produit m_etallique pour l'obtention d'objets lamin_es, moul_es ou autres, et proc_ed_es pour sa fabrication, France Patent 615147 1925.

[44] I. Duarte, J. Ferreira, Materials 2016, 9, 79.

[45] T. A. Schaedler, A. J. Jacobsen, A. Torrents, A. E. Sorensen, J. Lian, J. R. Greer, L. Valdevit, W. B. Carter, Science 2011, 334, 962.

[46] X. Zheng, H. Lee, T. H. Weisgraber, M. Shusteff, J. DeOtte, E. B. Duoss, J. D. Kuntz, M. M. Biener, Q. Ge, J. A. Jackson, Science 2014, 344, 1373.

[47] V. Zielasek, B. Jurgens, C. Schulz, J. Biener, M. M. Biener, A. V. Hamza, M. Bäumer, Angew. Chem. Int. Ed. 2006, 45, 8241.

[48] J. Biener,M.M. Biener, R. J. Madix, C. M. Friend, ACS Catal. 2015, 5, 6263.

[49] X. G. Wang, W. M. Wang, Z. Qi, C. C. Zhao, H. Ji, Z. H. Zhang, J. Alloys Compd. 2010, 508, 463.

[50] A. Wittstock, V. Zielasek, J. Biener, C.M. Friend, M. Bäumer, Science 2010, 327, 319.

[51] A. Wittstock, J. Biener, M. Bäumer, Phys. Chem. Chem. Phys. 2010, 12, 12919.

[52] C. Stenner, L.-H. Shao, N. Mameka, J. Weissmüller, Adv. Funct. Mater. 2016, 26, 5174.

[53] D. Kramer, R. N. Viswanath, J. Weissmüller, Nano Lett. 2004, 4, 793.

[54] H. J. Jin, J. Weissmüller, Adv. Eng. Mater. 2010, 12, 714.

[55] G. Tammann, Die chemischen und galvanischen Eigenschaften von Mischkristallreihen und ihre Atomverteilung ein Beitrag zur Kenntnis der Legierungen. Zeitschrift für anorganische und allgemeine Chemie 1919 (107) 1–239.

[56] G. Masing, Zeitschrift für anorganische und allgemeine Chemie 1921, 118, 293.

[57] P. R. Swann, Corrosion 1969, 25, 147.

[58] H. W. Pickering, C. Wagner, J. Electrochem. Soc. 1967, 114, 698. [

59] A. J. Forty, Nature 1979, 282, 597.

[60] K. Sieradzki, R. C. Newman, Philos. Mag. A 1985, 51, 95.

[61] R. C. Newman, K. Sieradzki, Science 1994, 263, 1708.

[62] J. Erlebacher, M. J. Aziz, A. Karma, N. Dimitrov, K. Sieradzki, Nature 2001, 410, 450.

[63] J. Erlebacher, J. Electrochem. Soc. 2004, 151, C614.

[64] K. Sieradzki, R. R. Corderman, K. Shukla, R. C. Newman, Philos. Mag. A 1989, 59, 713.

[65] T. Wada, K. Yubuta, A. Inoue, H. Kato, Mater. Lett. 2011, 65, 1076.

[66] K. Sieradzki, N. Dimitrov, D. Movrin, C. McCall, N. Vasiljevic, J. Erlebacher, J. Electrochem. Soc. 2002, 149, B370.

[67] R. C. Newman, S. G. Corcoran, J. Erlebacher,M. J. Aziz, K. Sieradzki, MRS Bull. 1999, 24, 24.

[68] I. C. Cheng, A. M. Hodge, Adv. Eng. Mater. 2012, 14, 219.

[69] M. Hakamada, M. Mabuchi, Crit. Rev. Solid State Mater. Sci. 2013, 38, 262.

[70] I. C. Cheng, A. M. Hodge, Scr. Mater. 2013, 69, 295.

[71] S. Shi, J. Markmann, J. Weissmüller, Philos. Mag. 2017, 97, 1571.

[72] Z. H. Zhang, Y. Wang, Z. Qi, W. H. Zhang, J. Y. Qin, J. Frenzel, J. Phys. Chem. C 2009, 113, 12629.

[73] I. McCue, E. Benn, B. Gaskey, J. Erlebacher, Annu. Rev. Mater. Res. 2016, 46, 263.

[74] A. M. Hodge, J. R. Hayes, J. A. Caro, J. Biener, A. V. Hamza, Adv. Eng. Mater. 2006, 8, 853.

[75] J. Snyder, P. Asanithi, A. B. Dalton, J. Erlebacher, Adv. Mater. 2008, 20, 4883.

[76] H. J. Jin, X. L. Wang, S. Parida, K. Wang, M. Seo, J. Weissmüller, Nano Lett. 2010, 10, 187.

[77] M. Graf, B. Roschning, J. Weissmüller, J. Electrochem. Soc. 2017, 164, C194.

[78] K. Wang, J. Weissmüller, Adv. Mater. 2013, 25, 1280.

[79] A. Wittstock, J. Biener, M. Bäumer, in Nanoporous Gold: From an Ancient Technology to a High-Tech Material, Royal Soc Chemistry, Cambridge 2012.

[80] X. Zheng, W. Smith, J. Jackson, B. Moran, H. Cui, D. Chen, J. Ye, N. Fang, N. Rodriguez, T. Weisgraber, C.M. Spadaccini, Nat. Mater. 2016, 15, 1100.

[81] Y. Ding, J. Erlebacher, J. Am. Chem. Soc. 2003, 125, 7772.

[82] G. W. Nyce, J. R. Hayes, A. V. Hamza, J. H. Satcher, Chem. Mater. 2007, 19, 344.

[83] Z. Qi, J. Weissmüller, ACS Nano 2013, 7, 5948.

[84] Z. Liu, P. C. Searson, J. Phys. Chem. B 2006, 110, 4318.

[85] T. Juarez, A. M. Hodge, Adv. Eng. Mater. 2016, 18, 65.

[86] C. X. Ji, P. C. Searson, J. Phys. Chem. B 2003, 107, 4494.

[87] C. X. Ji, P. C. Searson, Appl. Phys. Lett. 2002, 81, 4437.

[88] T. Y. Shin, S. H. Yoo, S. Park, Chem. Mat. 2008, 20, 5682.

[89] L. F. Liu, E. Pippel, R. Scholz, U. Gösele, Nano Lett. 2009, 9, 4352.

[90] S. Tominaka, J. Mater. Chem. 2011, 21, 9725.

[91] A. Chauvin, C. Delacote, L. Molina-Luna, M. Duerrschnabel, M. Boujtita, D. Thiry, K. Du, J. J. Ding, C. H. Choi, P. Y. Tessier, A. A. El Mel, ACS Appl. Mater. Interfaces 2016, 8, 6611.

[92] W. S. Chae, D. Van Gough, S. K. Ham, D. B. Robinson, P. V. Braun, ACS Appl. Mater. Interfaces 2012, 4, 3973.

[93] T. Fujita, Y. Kanoko, Y. Ito, L. Chen, A. Hirata, H. Kashani, O. Iwatsu, M. Chen, Adv. Sci. 2015, 2, 1500086.

[94] H. J. Qiu, Y. Ito, M. W. Chen, Scr. Mater. 2014, 89, 69.

[95] H. Bei, E. George, Acta. Mater. 2005, 53, 69.

[96] Q. Kong, L. Lian, Y. Liu, J. Zhang, L. Wang, W. Feng, Microporous Mesoporous Mater. 2015, 208, 152.

[97] Z. Qi, U. Vainio, A. Kornowski, M. Ritter, H. Weller, H. J. Jin, J. Weissmüller, Adv. Funct. Mater. 2015, 25, 2530.

[98] X. Wang, J. Frenzel, W. Wang, H. Ji, Z. Qi, Z. Zhang, G. Eggeler, J. Phys. Chem. C 2011, 115, 4456.

[99] H. Ji, X. Wang, C. Zhao, C. Zhang, J. Xu, Z. Zhang, CrystEngComm. 2011, 13, 2617.

[100] J. Yu, Y. Ding, C. Xu, A. Inoue, T. Sakurai, M. Chen, Chem. Mater. 2008, 20, 4548.

[101] H. J. Jin, D. Kramer, Y. Ivanisenko, J. Weissmüller, Adv. Eng. Mater. 2007, 9, 849.

[102] Q. Bai, Y. Wang, J. Zhang, Y. Ding, Z. Peng, Z. Zhang, J. Mater. Chem. C 2016, 4, 45.

[103] W. B. Liu, S. C. Zhang, N. Li, J. W. Zheng, Y. L. Xing, Microporous Mesoporous Mater. 2011, 138, 1.

[104] T. Song, M. Yan, Z. Shi, A. Atrens, M. Qian, Electrochim. Acta 2015, 164, 228.

[105] Z. H. Zhang, Y. Wang, Z. Qi, J. K. Lin, X. F. Bian, J. Phys. Chem. C 2009, 113, 1308.

[106] Z. Zhang, Y. Wang, Z. Qi, C. Somsen, X. Wang, C. Zhao, J. Mater. Chem. 2009, 19, 6042.

[107] X. Wang, J. Sun, C. Zhang, T. Kou, Z. Zhang, J. Phys. Chem. C 2012, 116, 13271.

[108] H. Duan, Q. Hao, C. Xu, J. Power Sources 2015, 280, 483.

[109] D. Zhao, D. Fan, J. Wang, C. Xu, Microchim. Acta 2015, 182, 1345.

[110] Z. H. Dan, F. X. Qin, Y. Sugawara, I. Muto, N. Hara, Intermetallics 2012, 31, 157.

[111] C. Xu, Q. Li, Y. Liu, J. Wang, H. Geng, Langmuir 2012, 28, 1886.

[112] J. Hou, C. Xu, D. Zhao, J. Zhou, Sens. Actuators B 2016, 225, 241.

[113] M. E. Cox, D. C. Dunand, Mater. Sci. Eng. A 2011, 528, 2401.

[114] Y. W. Zhan, S. S. Zeng, H. D. Bian, Z. Li, Z. T. Xu, J. Lu, Y. Y. Li, Nano Res. 2016, 9, 2364.

[115] V. Shapovalov, L. Boyko, Adv. Eng. Mater. 2004, 6, 407.

[116] X. Zhang, Y. Li, Y. Liu, H. Zhang, Mater. Lett. 2013, 92, 448.

[117] X. Zhang, Y. Li, H. Zhang, Y. Liu, Mater. Lett. 2013, 106, 417.

[118] S. Parida, D. Kramer, C. A. Volkert, H. Rösner, J. Erlebacher, J. Weissmüller, Phys. Rev. Lett. 2006, 97, 035504.

[119] S. V. Petegem, S. Brandstetter, R. Maass, A. M. Hodge, B. S. El- Dasher, J. Biener, B. Schmitt, C. Borca, H. V. Swygenhoven, Nano Lett. 2009, 9, 1158.

[120] Y. Sun, T. J. Balk, Scr. Mater. 2008, 58, 727.

[121] Y. Zhong, J. Markmann, H.-J. Jin, Y. Ivanisenko, L. Kurmanaeva, J. Weissmüller, Adv. Eng. Mater. 2014, 16, 389.

[122] E. Detsi, S. Punzhin, J. Rao, P. R. Onck, J. T. M. De Hosson, ACS Nano 2012, 6, 3734.

[123] M. M. Biener, J. Biener, A. Wichmann, A. Wittstock, T. F. Baumann, M. Bäumer, A. V. Hamza, Nano Lett. 2011, 11, 3085.

[124] J. Shan, N. Janvelyan, H. Li, J. Liu, T. M. Egle, J. Ye, M. M. Biener, J. Biener, C. M. Friend, M. Flytzani-Stephanopoulos, Appl. Catal. B 2017, 205, 541.

[125] Y. Ding, M. W. Chen, J. Erlebacher, J. Am. Chem. Soc. 2004, 126, 6876.

[126] X. Lang, A. Hirata, T. Fujita, M. Chen, Nat. Nanotechnol. 2011, 6, 232.

[127] S. H. Yoo, S. Park, Adv. Mater. 2007, 19, 1612.

[128] S. Park, P. X. Yang, P. Corredor,M. J. Weaver, J. Am. Chem. Soc. 2002, 124, 2428.

[129] R. Y. Wang, C. Wang, W. B. Cai, Y. Ding, Adv. Mater. 2010, 22, 1845.

[130] A. Kiani, E. N. Fard, Electrochim. Acta 2009, 54, 7254.

[131] Y. Wang, W. Huang, C. Si, J. Zhang, X. Yan, C. Jin, Y. Ding, Z. Zhang, Nano Res. 2016, 9, 3781.

[132] X. J. Yan, H. Y. Xiong, Q. G. Bai, J. Frenzel, C. H. Si, X. T. Chen, G. Eggeler, Z. H. Zhang, RSC Adv. 2015, 5, 19409.

[133] L. Y. Chen, T. Fujita, Y. Ding, M. W. Chen, Adv. Funct. Mater. 2010, 20, 2279.

[134] C. X. Xu, L. Q. Wang, R. Y. Wang, K. Wang, Y. Zhang, F. Tian, Y. Ding, Adv. Mater. 2009, 21, 2165.

[135] X. Y. Lang, L. Zhang, T. Fujita, Y. Ding, M. W. Chen, J. Power Sources 2012, 197, 325.

[136] E. Detsi, P. R. Onck, J. T. M. De Hosson, Appl. Phys. Lett. 2013, 103, 193101.

[137] S. Sattayasamitsathit, A. M. O'Mahony, X. Xiao, S. M. Brozik, C. M. Washburn, D. R. Wheeler, W. Gao, S. Minteer, J. Cha, D. B. Burckel, R. Polsky, J. Wang, J. Mater. Chem. 2012, 22, 11950.

[138] X. Ke, Y. Xu, C. Yu, J. Zhao, G. Cui, D. Higgins, Q. Li, G. Wu, J. Power Sources 2014, 269, 461.

[139] X. Ke, Y. Xu, C. Yu, J. Zhao, G. Cui, D. Higgins, Z. Chen, Q. Li, H. Xu, G. Wu, J. Mater. Chem. A 2014, 2, 16474.

[140] M. C. Dixon, T. A. Daniel, M. Hieda, D. M. Smilgies, M. H. W. Chan, D. L. Allara, Langmuir 2007, 23, 2414.

[141] L.-H. Qian, Y. Ding, T. Fujita, M.-W. Chen, Langmuir 2008, 24, 4426.

[142] D. Jalas, L.-H. Shao, R. Canchi, T. Okuma, S. Lang, A. Petrov, J. Weissmüller, M. Eich, Sci. Rep. 2017, 7, 44139.

[143] Y. H. Xue, J. Markmann, H. L. Duan, J. Weissmuller, P. Huber, Nat. Commun. 2014, 5, 4327.

[144] H. Oppermann, L. Dietrich, Microelectron. Reliab. 2012, 52, 356.

[145] C. A. R. Chapman, H. Chen, M. Stamou, P. J. Lein, E. Seker, Cell. Mol. Bioeng. 2016, 9, 433.

[146] C. A. Chapman, H. Chen, M. Stamou, J. Biener, M. M. Biener, P. J. Lein, E. Seker, ACS Appl. Mater. Interfaces 2015, 7, 7093.

[147] C. A. R. Chapman, L. Wang, H. Chen, J. Garrison, P. J. Lein, E. Seker, Adv. Funct. Mater. 2017, 27, 1604631.

[148] I. V. Okulov, J. Weissmüller, J. Markmann, Sci. Rep. 2017, 7, 20.

[149] N. Kobayashi, T. Sakumoto, S. Mori, H. Ogata, K. C. Park, K. Takeuchi, M. Endo, Electrochim. Acta 2013, 105, 455.

[150] Y.-J. Lee, D.-J. Park, J.-Y. Park, Y. Kim, Sensors 2008, 8, 6154.

[151] D. Liu, Z. Yang, P. Wang, F. Li, D. Wang, D. He, Nanoscale 2013, 5, 1917.

[152] Z. Qi, J. Weissmüller, ACS Nano 2013, 7, 5948.

[153] J. Weissmüller, J. W. Cahn, Acta. Mater. 1997, 45, 1899.

[154] J. Weissmüller, R. N. Viswanath, D. Kramer, P. Zimmer, R. Würschum, H. Gleiter, Science 2003, 300, 312.

[155] J. Biener, A. Wittstock, L. A. Zepeda-Ruiz, M. M. Biener, V. Zielasek, D. Kramer, R. N. Viswanath, J. Weissmüller, M. Bäumer, A. V. Hamza, Nat. Mater. 2009, 8, 47.

[156] W. Haiss, Rep. Prog. Phys. 2001, 64, 591.

[157] F. Weigend, J. Weissmüller, F. Evers, Small 2006, 2, 1497.

[158] E. Detsi, M. S. Selles, P. R. Onck, J. T. M. De Hosson, Scr. Mater. 2013, 69, 195.

[159] R. N. Viswanath, J. Weissmüller, Acta. Mater. 2013, 61, 6301.

[160] J. Weissmüller, D. Kramer, Langmuir 2005, 21, 4592.

[161] A. Y. Gokhshtein, Dokl. Akad. Nauk SSSR 1969, 187, 601.

[162] M. Smetanin, D. Kramer, S. Mohanan, U. Herr, J. Weissmüller, Phys. Chem. Chem. Phys. 2009, 11, 9008.

[163] C. Cheng, A. H. W. Ngan, ACS Nano 2015, 9, 3984.

[164] C. Cheng, J. Weissmüller, A. H.W. Ngan, Adv. Mater. 2016, 28, 5315.

[165] J. Zhang, Y. Wang, C. Si, Q. Bai, W. Ma, H. Gao, Z. Zhang, Electrochim. Acta 2016, 220, 91.

[166] J. Zhang, Q. Bai, Z. Zhang, Nanoscale 2016, 8, 7287.

[167] B. Sharma, R. R. Frontiera, A.-I. Henry, E. Ringe, R. P. Van Duyne, Mater. Today 2012, 15, 16.

[168] S. O. Kucheyev, J. R. Hayes, J. Biener, T. Huser, C. E. Talley, A. V. Hamza, Appl. Phys. Lett. 2006, 89, 053102.

[169] X. Y. Lang, L. Y. Chen, P. F. Guan, T. Fujita, M. W. Chen, Appl. Phys. Lett. 2009, 94, 213109.

[170] L. H. Qian, X. Q. Yan, T. Fujita, A. Inoue, M. W. Chen, Appl. Phys. Lett. 2007, 90, 153102.

[171] L. H. Qian, B. Das, Y. Li, Z. L. Yang, J. Mater. Chem. 2010, 20, 6891.

[172] L. Zhang, X. Y. Lang, A. Hirata, M. W. Chen, ACS Nano 2011, 5, 4407.

[173] X. Zhang, Y. Zheng, X. Liu, W. Lu, J. Dai, D. Y. Lei, D. R. MacFarlane, Adv. Mater. 2015, 27, 1090.

[174] L. Y. Chen, J. S. Yu, T. Fujita, M. W. Chen, Adv. Funct. Mater. 2009, 19, 1221.

[175] X. Ke, Z. Li, L. Gan, J. Zhao, G. Cui, W. Kellogg, D. Matera, D. Higgins, G. Wu, Electrochim. Acta 2015, 170, 337.

[176] D. Zhao, G. Yu, K. Tian, C. Xu, Biosens. Bioelectron. 2016, 82, 119.

[177] A. J. Smith, D. L. Trimm, Annu. Rev. Mater. Res. 2005, 35, 127.

[178] C. G. Freyschlag, R. J. Madix, Mater. Today 2011, 14, 134.

[179] B. Zugic, L. Wang, C. Heine, D. N. Zakharov, B. A. Lechner, E. A. Stach, J. Biener, M. Salmeron, R. J. Madix, C. M. Friend, Nat. Mater. 2017, 16, 558.

[180] A. Kucernak, J. H. Jiang, Chem. Eng. J. 2003, 93, 81.

[181] X. Wang, W. Wang, Z. Qi, C. Zhao, H. Ji, Z. Zhang, J. Power Sources 2010, 195, 6740.

[182] J. Xu, C. Zhang, X. Wang, H. Ji, C. Zhao, Y. Wang, Z. Zhang, Green Chem. 2011, 13, 1914.

[183] X.-Y. Lang, G.-F. Han, B.-B. Xiao, L. Gu, Z.-Z. Yang, Z. Wen, Y.-F. Zhu, M. Zhao, J.-C. Li, Q. Jiang, Adv. Funct. Mater. 2015, 25, 230.

[184] H. Ji, J. Frenzel, Z. Qi, X. Wang, C. Zhao, Z. Zhang, G. Eggeler, CrystEngComm 2010, 12, 4059.

[185] D. Wang, P. Schaaf, J. Mater. Chem. 2012, 22, 5344.

[186] M. Oezaslan, M. Heggen, P. Strasser, J. Am. Chem. Soc. 2011, 134, 514.

[187] J. Snyder, I. McCue, K. Livi, J. Erlebacher, J. Am. Chem. Soc. 2012, 134, 8633.

[188] D. Wang, P. Zhao, Y. Li, Sci. Rep. 2011, 1, 37.

[189] J. T. Zhang, P. P. Liu, H. Y. Ma, Y. Ding, J. Phys. Chem. C 2007, 111, 10382.

[190] C. X. Xu, J. X. Su, X. H. Xu, P. P. Liu, H. J. Zhao, F. Tian, Y. Ding, J. Am. Chem. Soc. 2007, 129, 42.

[191] R. Zeis, T. Lei, K. Sieradzki, J. Snyder, J. Erlebacher, J. Catal. 2008, 253, 132.

[192] M. L. Personick, B. Zugic, M. M. Biener, J. Biener, R. J. Madix, C. M. Friend, ACS Catal. 2015, 5, 4237.

[193] J. Snyder, J. Erlebacher, ECS Trans. 2011, 41, 1021.

[194] R. Zeis, A. Mathur, G. Fritz, J. Lee, J. Erlebacher, J. Power Sources 2007, 165, 65.

[195] J. T. Zhang, H. Y. Ma, D. J. Zhang, P. P. Liu, F. Tian, Y. Ding, Phys. Chem. Chem. Phys. 2008, 10, 3250.

[196] S. Xiao, F. Xiao, Y. Hu, S. Yuan, S. Wang, L. Qian, Y. Liu, Sci. Rep. 2014, 4, 4370.

[197] L. F. Liu, R. Scholz, E. Pippel, U. Gösele, J. Mater. Chem. 2010, 20, 5621.

[198] L. F. Liu, Z. P. Huang, D. A. Wang, R. Scholz, E. Pippel, Nanotechnology 2011, 22, 105604.

[199] J. I. Shui, C. Chen, J. C. M. Li, Adv. Funct. Mater. 2011, 21, 3357.

[200] C. C. Jia, H. M. Yin, H. Y. Ma, R. Y. Wang, X. B. Ge, A. Q. Zhou, X. H. Xu, Y. Ding, J. Phys. Chem. C 2009, 113, 16138.

[201] X. Guo, J. Han, P. Liu, L. Chen, Y. Ito, Z. Jian, T. Jin, A. Hirata, F. Li, T. Fujita, N. Asao, H. Zhou, M. Chen, Sci. Rep. 2016, 6, 33466.

[202] K. Mizushima, P. C. Jones, P. J. Wiseman, J. B. Goodenough, Mater. Res. Bull. 1980, 15, 783.

[203] Y. Yu, L. Gu, X. Y. Lang, C. B. Zhu, T. Fujita, M. W. Chen, J. Maier, Adv. Mater. 2011, 23, 2443.

[204] S. Zhang, Y. Xing, T. Jiang, Z. Du, F. Li, L. He, W. Liu, J. Power Sources 2011, 196, 6915.

[205] C. Hou, X.-Y. Lang, G.-F. Han, Y.-Q. Li, L. Zhao, Z. Wen, Y.-F. Zhu, M. Zhao, J.-C. Li, J.-S. Lian, Q. Jiang, Sci. Rep. 2013, 3, 2878.

[206] J. Ye, A. C. Baumgaertel, Y. M. Wang, J. Biener, M. M. Biener, ACS Nano 2015, 9, 2194.

[207] M. S. Halper, J. C. Ellenbogen, Supercapacitors: A Brief Overview, MITRE Nanosystems Group, Virginia 2006.

[208] X. Y. Lang, H. T. Yuan, Y. Iwasa, M. W. Chen, Scr. Mater. 2011, 64, 923.

[209] X. Yang, C. Cheng, Y. Wang, L. Qiu, D. Li, Science 2013, 341, 534.

[210] A. Burke, Electrochim. Acta 2007, 53, 1083.

[211] F. Meng, Y. Ding, Adv. Mater. 2011, 23, 4098.

[212] Y. Hou, L. Chen, P. Liu, J. Kang, T. Fujita, M. Chen, J. Mater. Chem. A 2014, 2, 10910.

[213] Z. Zeng, X. Long, H. Zhou, E. Guo, X. Wang, Z. Hu, Electrochim. Acta 2015, 163, 107.

[214] A. Halder, S. Patra, B. Viswanath, N. Munichandraiah, N. Ravishankar, Nanoscale 2011, 3, 725.

[215] C. Cheng, A. H. Ngan, ACS Nano 2015, 9, 3984.

[216] X.-F. Xing, D.-Q. Han, Y.-F. Wu, Y. Guan, N. Bao, X.-H. Xu, Mater. Lett. 2012, 71, 108.

[217] X. Ge, R. Wang, P. Liu, Y. Ding, Chem. Mat. 2007, 19, 5827.